

Reconstruction of the 1941 GLOF process chain at Lake Palcacocha (Cordillera Blanca, Perú)

Martin Mergili, Shiva P. Pudasaini, Adam Emmer, Jan-Thomas Fischer, Alejo Cochachin, and Holger Frey

Response to the comments of Referee #1 (John Reynolds)

We would like to thank the reviewer for the constructive remarks. Below, we address each comment in full detail. Our response is written in blue colour. Changes in the manuscript are highlighted in yellow colour.

This is an interesting and useful paper that serves two important functions. Firstly, it provides a back analysis of the 1941 GLOF process chain from Laguna Palcacocha, Peru, that helps an understanding of the physical processes associated with the event. Secondly, it is a useful demonstration of r.avaflow software that is fast becoming more widely applied for such studies. The only comment I would make in this discussion is to expand a little on the detail behind the Laguna 513 situation between 1988 and 1994 as many papers that cite this lake do not report the full story and it merits telling again. Details of the remediation work undertaken have been described by *Reynolds, J.M. 1998. Managing the risks of glacial flooding at hydro plants. Hydro Review Worldwide, 6(2):18-22*; and by *Reynolds, J.M., Dolecki, A. and Portocarrero, C. 1998. The construction of a drainage tunnel as part of glacial lake hazard mitigation at Hualcán, Cordillera Blanca, Peru. In: Maund, J. & Eddleston, M. (eds.) Geohazards in engineering geology. Geological Society Engineering Group Special Publication No. 15, pp. 41-48.*

In essence, in late 1988, surveying undertaken by local engineers identified that the small moraine dam impounding Lake 513 was ice cored and that this ice core was subsiding through ablation by ~11 cm/month. It was a simple calculation, therefore, to estimate that by early 1989, the subsidence would have reduced the freeboard to zero and worse, would have resulted in the moraine dam failing and being eroded leading to an outburst flood. The local engineers, led by Cesar Portocarrero, identified that siphoning would be sufficient and practical to reduce the lake level by 3 m or so to alleviate a possible outburst. However, they had insufficient funds to purchase the necessary siphons. Two days before Christmas 1988, Cesar phoned me in the UK from Peru to ask if I could help. A few phone calls and several hours later I had managed to persuade the British Embassy in Lima to provide the necessary funds. Consequently, within a couple of weeks the siphons had been installed and the lake level lowered. In 1991, a small ice avalanche, thought to have originated from the hanging glacier perched above the lake, fell into the lake producing a small displacement wave. However, this was sufficient to breach the remains of the moraine dam and produce a small outburst flood. It had the consequences of lowering the water level down to and exposed a solid rock bar that had been beneath the terminal moraine dam. The new water level was by this time only just below the rim of the rock bar. Ing. Portocarrero began to design a more permanent mitigation scheme of tunneling through the rock bar to lower the lake by 20 m. In 1993, having been informed of his design, it became apparent that the water hydrostatic pressure under 20 m plus head of water could rupture the discharge portal end of the proposed tunnel leading to a greater failure of the distal flank of the rock bar. With emergency funding provided by the British Government, in late 1993 Reynolds and Dolecki visited the site operations with Ing. Portocarrero. We came up with a scheme for which the equipment was already on site that required the excavation of a tiered suite of tunnels whose inflow portals were set 5 m vertically apart, with the uppermost tunnel

being opened first, to lower the lake level down by 5 m; then the second tunnel, for a further 5 m lowering. Explosives failed to detonate for the break through for the third tunnel, so it was decided to go for a 10m breach through to the lowermost tunnel, which was established safely and the lake was successfully lowered by 20 m, thereby creating a freeboard against avalanche push waves and displacement waves in the case of further avalanche activity. The thinking at that time was that an ice avalanche would most probably originate from the ice cliff associated with the perched hanging glacier immediately above the upstream end of the lake. The rock/ice avalanche that occurred in 2010 was from the uppermost flanks of the back wall above the lake. This was then when it was realised that this avalanche might have been triggered by thawing of permafrost where the rock face was exposed. Thankfully, having lowered the lake level by May 1994 by 20 m, when the avalanche occurred in 2010, the exposed rock bar with 20 m of freeboard accommodated most of the 28-m high avalanche push wave, with only a residual amount overtopping the rock bar. Had the further remediation not have been undertaken, the consequences of this 2010 would most likely have been far more tragic, with possibly as many as 5-6,000 fatalities, as defined by the local mayor. Whilst the 2010 GLOF/alluvion caused damage, especially to the outskirts of the town, there were no casualties.

We are very glad to see that the reviewer likes our paper. We have included the 2010 event at Laguna 513 in the introduction and the discussion of the revised manuscript, referring to the suggested literature. We have kept the text blocks concerning Laguna 513 brief and concise, clearly relating them to those aspects also relevant for the present work. A more detailed account of the remediation measures and the 2010 event would be out of scope here, but could be of great interest for a future study. In the revised manuscript, we have mainly added the following pieces of text:

Introduction (L64-66):

Most notably, lowering the lake level of Laguna 513 through a system of tunnels in the 1990s has probably prevented a disaster downstream when a rock-ice avalanche impacted that lake in 2010 (Reynolds, 1998; Reynolds et al., 1998; Schneider et al., 2014).

Discussion (L486-490):

In principle, such an understanding can be transferred to present hazardous situations in order to inform the design of technical remediation measures. Earlier, measures were not only implemented at Lake Palcacocha (Portocarrero, 2014), but also at various other lakes such as Laguna 513: a tunnelling scheme implemented in the 1990s strongly reduced the impacts of the 2010 GLOF process chain (Reynolds, 1998; Reynolds et al., 1998; Schneider et al., 2014).

Reconstruction of the 1941 GLOF process chain at Lake Palcacocha (Cordillera Blanca, Perú)

Martin Mergili^{1,2}, Shiva P. Pudasaini³, Adam Emmer⁴, Jan-Thomas Fischer⁵, Alejo Cochachin⁶, and Holger Frey⁷

¹ Institute of Applied Geology, University of Natural Resources and Life Sciences (BOKU), Peter-Jordan-Straße 82, 1190 Vienna, Austria

² Geomorphological Systems and Risk Research, Department of Geography and Regional Research, University of Vienna, Universitätsstraße 7, 1010 Vienna, Austria

³ Geophysics Section, **Institute of Geosciences**, University of Bonn, Meckenheimer Allee 176, 53115 Bonn, Germany

⁴ Department of the Human Dimensions of Global Change, Global Change Research Institute, The Czech Academy of Sciences, Bělidla 986/4a, 603 00, Brno, Czech Republic

⁵ Department of Natural Hazards, Austrian Research Centre for Forests (BFW), Rennweg 1, 6020 Innsbruck, Austria

⁶ Unidad de Glaciología y Recursos Hídricos, Autoridad Nacional del Agua, Confraternidad Internacional 167, Huaráz, Perú

⁷ Department of Geography, University of Zurich, Winterthurerstrasse 190, 8057 Zurich, Switzerland

Correspondence to: M. Mergili (martin.mergili@boku.ac.at)

Abstract

The Cordillera Blanca in Perú has been the scene of rapid deglaciation for many decades. One of numerous lakes formed in the front of the retreating glaciers is the moraine-dammed Lake Palcacocha, which drained suddenly due to an unknown cause in 1941. The resulting Glacial Lake Outburst Flood (GLOF) led to dam failure and complete drainage of Lake Jircacocha downstream, and to major destruction and thousands of fatalities in the city of Huaráz at a distance of 23 km. We chose an integrated approach to revisit the 1941 event in terms of topographic reconstruction and numerical back-calculation with the GIS-based open source mass flow/process chain simulation framework r.avaflow. Thereby we consider four scenarios: (A) and (AX) breach of the moraine dam of Lake Palcacocha due to retrogressive erosion, assuming two different fluid characteristics; (B) failure of the moraine dam caused by the impact of a landslide onto the lake; and (C) geomechanical failure and collapse of the moraine dam. The simulations largely yield empirically adequate results with physically plausible parameters, taking the documentation of the 1941 event and previous calculations of future scenarios as reference. Most simulation scenarios indicate travel times between 36 and 70 minutes to reach Huaráz, accompanied with peak discharges above 10,000 m³/s. The results of the scenarios indicate that the most likely initiation mechanism would be retrogressive erosion, possibly triggered by a minor impact wave and/or facilitated by a weak stability condition of the moraine dam. However, the involvement of Lake Jircacocha disguises part of the signal of process initiation farther downstream. Predictive simulations of possible future events have to be based on a larger set of back-calculated GLOF process chains, taking into account the expected parameter uncertainties and appropriate strategies to deal with critical threshold effects.

Keywords: GLOF, high-mountain lakes, Lake Palcacocha, numerical simulation, process chain, r.avaflow, two-phase flows

1 Introduction

Glacial retreat in high-mountain areas often leads, after some lag time (Harrison et al., 2018), to the formation of proglacial lakes, which are impounded by moraine dams or bedrock swells. Such lakes may drain suddenly, releasing a large amount of water which may result in complex and potentially catastrophic process chains downstream. Glacial lakes and outburst floods (GLOFs) have been subject of numerous studies covering many mountain regions all around the globe (Hewitt, 1982; Haeberli, 1983; Richardson and Reynolds, 2000; Huggel et al., 2003; Breien et al., 2008; Hewitt and Liu, 2010; Bolch et al., 2011; Mergili and Schneider, 2011; Mergili et al., 2013; Clague and O'Connor, 2014; Emmer et al., 2015, 2016; Sattar et al., 2019a, b; Turzewski et al., 2019).

The Cordillera Blanca (Perú) represents the most glacierized mountain chain of the Tropics. Glacial lakes and GLOFs are particularly common there (Carey, 2005). 882 high-mountain lakes were identified by Emmer et al. (2016). Some of these lakes are susceptible to GLOFs (Vilímek et al., 2005; Emmer and Vilímek, 2013, 2014; ANA, 2014; Iturrizaga, 2014). A total of 28 geomorphologically effective GLOFs originating from moraine-dammed lakes have been documented (Emmer, 2017). Most recently, GLOFs were recorded at Lake Safuna Alta (2002 – the trigger was a rock avalanche into the lake; Hubbard et al., 2005), at Lake Palcacocha (2003 – landslide-induced overtopping of the dam; Vilímek et al., 2005), and at Lake 513 (2010 – triggered by an ice avalanche; Carey et al., 2012). Lake Artizón Alto was hit by a landslide from a moraine in 2012, which resulted in cascading effects involving three more lakes and entrainment of a considerable amount of debris in the Artizón Valley and, farther downstream, the Santa Cruz Valley (Mergili et al., 2018a). A pronounced peak in frequency of high-magnitude GLOFs, however, was already observed in the 1940s and 1950s, when lakes of notable size had formed behind steep terminal moraine walls (Emmer et al., 2019). The most prominent and well-documented GLOF in this period occurred on 13 December 1941, when Lake Palcacocha in the Quilcay Catchment drained suddenly, leading to a process chain that resulted in at least 1600 fatalities and major destruction in the town of Huaráz 23 km downstream (Broggi, 1942; Oppenheim, 1946; Concha, 1952; Wegner, 2014).

In the Cordillera Blanca, the local population is highly vulnerable to high-mountain process chains, often induced by GLOFs (Carey, 2005; Hofflinger et al., 2019). In order to mitigate this threat, tens of lakes in the Cordillera Blanca have been remediated through technical measures such as open cuts, artificial dams or tunnels during the last decades (Oppenheim, 1946; Zapata 1978; Portocarrero, 1984; Carey, 2005; Portocarrero, 2014; Emmer et al., 2018). Most notably, lowering the lake level of Laguna 513 through a system of tunnels in the 1990s has probably prevented a disaster downstream when a rock-ice avalanche impacted that lake in 2010 (Reynolds, 1998; Reynolds et al., 1998; Schneider et al., 2014). However, the management of GLOF risk is a difficult task (Carey et al., 2014). Anticipation of the impact area and magnitude of GLOF cascades – and, as a consequence, also hazard mapping and the design of technical remediation measures – relies to a large extent on the application of computational mass flow models (GAPHAZ, 2017). Important progress was made since the mid-20th Century: various models were developed, and have more recently been implemented in simulation software tools (Voellmy, 1955; Savage and Hutter, 1989; Iverson, 1997; Takahashi et al., 2002; Pitman and Le, 2005; McDougall and Hungr, 2004; Pudasaini and Hutter, 2007; Chisolm and McKinney, 2018). Most of these approaches represent single-phase mixture models. Tools like RAMMS (Christen et al., 2010) or FLO-2D were used for the simulation of GLOFs (Mergili et al., 2011). Schneider et al. (2014), Wormi et al. (2014), and Somos-Valenzuela et al. (2016) have sequentially coupled two or more tools for simulating landslide – GLOF cascades. However, single-phase models do not describe the interactions between the solid and the fluid phase, or dynamic landslide-lake interactions, in an appropriate way, so that workarounds are necessary (Gabl et al., 2015). Wormi et al. (2014) called for integrated approaches. They would have to build on two- or even three-phase models considering water, debris, and ice separately, but also the interactions between the phases and the

79 flow transformations. Pudasaini (2012) introduced a general two-phase flow model considering mixtures of solid parti-
80 cles and viscous fluid which has been used for the simulation of computer-generated examples of sub-aqueous land-
81 slides and particle transport (Kafle et al., 2016, 2019) as well as GLOFs (Kattel et al., 2016).

82 The recently introduced open source GIS simulation framework *r.avaflow* (Mergili et al., 2017) applies an extended
83 version of the approach of Pudasaini (2012). It was used to back-calculate the 2012 Santa Cruz process chain involving
84 four lakes (Mergili et al., 2018a), and the 1962 and 1970 Huascarán landslides (Mergili et al., 2018b), both in the Cor-
85 dillera Blanca. These studies identified the capability of that tool to appropriately simulate the transformations at the
86 boundary of individual processes, where one process transforms to the next, as one of the major challenges. Open is-
87 sues include the proper understanding of wave generation as a response to landslides impacting high-mountain lakes
88 and, as a consequence, the quantification of essential parameters such as the volume of overtopping water and the
89 discharge (Westoby et al., 2014). Further, uncertainties in the model parameters and the initial conditions accumulate
90 at process boundaries (Schaub et al. 2016), and threshold effects are expected to result in strongly non-linear responses
91 of the model error (Mergili et al., 2018a, b). In high-energy mass flows, the physical characteristics of the processes
92 involved are not always understood at the required level of detail (Mergili et al., 2018b).

93 On the one hand, flow models and simulation tools can help us to better understand some of the key mechanisms of
94 high-mountain process chains. On the other hand, well documented case studies are important to gain a better under-
95 standing on which questions can be tackled with simulation tools, and which questions cannot be answered without
96 further research. In the present work, we explore this field of uncertainty by applying the *r.avaflow* computational
97 tool to the 1941 Lake Palcacocha GLOF process chain. Thereby, based on the simulation of different scenarios, we
98 investigate on the following research questions:

- 99 1. What is the most likely release mechanism of initiating the process chain of the 1941 GLOF of Lake Palcaco-
100 cha?
- 101 2. Are we able to back-calculate this process chain in an empirically adequate way with physically plausible
102 model parameters? Mergili et al. (2018b) reported a trade-off between these two criteria for the simulation of
103 the 1970 Huascarán landslide.
- 104 3. What are the major challenges in achieving successful (empirically adequate and physically plausible) simula-
105 tions?
- 106 4. What can we learn with regard to forward calculations of possible future events?

107 In Sect. 2 we depict the local conditions and the documentation of the event. After having introduced the computa-
108 tional framework *r.avaflow* (Sect. 3), we describe in detail the simulation input (Sect. 4) and our findings (Sect. 5). We
109 discuss the results (Sect. 6) and finally summarize the key points of the research (Sect. 7).

110 **2 Lake Palcacocha**

111 **2.1 Quilcay catchment and Cojup Valley**

112 Lake Palcacocha is part of a proglacial system in the headwaters of the Cojup Valley in the Cordillera Blanca, Perú
113 (Fig. 1). This system was – and is still – shaped by the glaciers originating from the southwestern slopes of Nevado
114 Palcaraju (6,264 m a.s.l.) and Nevado Pucaranra (6,156 m a.s.l.). A prominent horseshoe-shaped ridge of lateral and
115 terminal moraines marks the extent of the glacier during the first peak of the Little Ice Age, dated using lichenometry
116 to the 17th Century (Emmer, 2017). With glacier retreat, the depression behind the moraine ridge was filled with a

lake, named Lake Palcacocha. A photograph taken by Hans Kinzl in 1939 (Kinzl and Schneider, 1950) indicates a lake level of 4,610 m a.s.l., allowing surficial outflow (Fig. 2a). Using this photograph, Vilímek et al. (2005) estimated a lake volume between 9 and 11 million m³ at that time, whereas an unpublished estimate of the Autoridad Nacional del Agua (ANA) arrived at approx. 13.1 million m³. It is assumed that the situation was essentially the same at the time of the 1941 GLOF (Sect. 2.2).

The Cojup Valley is part of the Quilcay catchment, draining towards southwest to the city of Huaráz, capital of the department of Ancash located at 3,090 m a.s.l. at the outlet to the Río Santa Valley (Callejon de Huaylas). The distance between Lake Palcacocha and Huaráz is approx. 23 km, whereas the vertical drop is approx. 1,500 m. The Cojup Valley forms a glacially shaped high-mountain valley in its upper part whilst cutting through the promontory of the Cordillera Blanca in its lower part. 8 km downstream from Lake Palcacocha (15 km upstream of Huaráz), the landslide-dammed Lake Jircacocha (4.8 million m³; Vilímek et al., 2005) existed until 1941 (Andres et al., 2018). The remnants of this lake are still clearly visible in the landscape in 2017, mainly through the change in vegetation and the presence of fine lake sediments (Fig. 2b). Table 1 summarizes the major characteristics of Lake Palcacocha and Lake Jircacocha before the 1941 GLOF.

2.2 1941 multi-lake outburst flood from Lake Palcacocha

On 13 December 1941 part of the city of Huaráz was destroyed by a catastrophic GLOF-induced debris and mud flow, with thousands of fatalities. Portocarrero (1984) gives a number of 4000 deaths, Wegner (2014) a number of 1800; but this type of information has to be interpreted with care (Evans et al., 2009). The disaster was the result of a multi-lake outburst flood in the upper part of the Cojup Valley. Sudden breach of the dam and the drainage of Lake Palcacocha (Figs. 2c and e) led to a mass flow proceeding down the valley. Part of the eroded dam material, mostly coarse material, blocks and boulders, was deposited directly downstream from the moraine dam, forming an outwash fan typical for moraine dam failures (Fig. 2c), whereas additional solid material forming the catastrophic mass flow was most likely eroded further along the flow path (both lateral and basal erosion were observed; Wegner, 2014). The impact of the flow on Lake Jircacocha led to overtopping and erosion of the landslide dam down to its base, leading to the complete and permanent disappearance of this lake. The associated uptake of the additional water and debris increased the energy of the flow, and massive erosion occurred in the steeper downstream part of the valley, near the city of Huaráz. Reports by the local communities indicate that the valley was deepened substantially, so that the traffic between villages was interrupted. According to Somos-Valenzuela et al. (2016), the valley bottom was lowered by as much as 50 m in some parts.

The impact area of the 1941 multi-GLOF and the condition of Lake Palcacocha after the event are well documented through aerial imagery acquired in 1948 (Fig. 3). The image of Hans Kinzl acquired in 1939 (Fig. 2a) is the only record of the status before the event. Additional information is available through eyewitness reports (Wegner, 2014). However, as Lake Palcacocha is located in a remote, uninhabited area, no direct estimates of travel times or associated flow velocities are available. Also the trigger of the sudden drainage of Lake Palcacocha remains unclear. Two mechanisms appear most likely: (i) retrogressive erosion, possibly triggered by an impact wave related to calving or an ice avalanche, resulting in overtopping of the dam (however, Vilímek et al., 2005 state that there are no indicators for such an impact); or (ii) internal erosion of the dam through piping, leading to the failure.

2.3 Lake evolution since 1941

As shown on the aerial images from 1948, Lake Palcacocha was drastically reduced to a small remnant proglacial pond, impounded by a basal moraine ridge within the former lake area, at a water level of 4563 m a.s.l., 47 m lower than

157 before the 1941 event (Fig. 3a). However, glacial retreat during the following decades led to an increase of the lake
158 area and volume (Vilímek et al., 2005). After reinforcement of the dam and the construction of an artificial drainage in
159 the early 1970s, a lake volume of 514,800 m³ was derived from bathymetric measurements (Ojeda, 1974). In 1974, two
160 artificial dams and a permanent drainage channel were installed, stabilizing the lake level with a freeboard of 7 m to
161 the dam crest (Portocarrero, 2014). By 2003, the volume had increased to 3.69 million m³ (Zapata et al., 2003). In the
162 same year, a landslide from the left lateral moraine caused a minor flood wave in the Cojup Valley (Fig. 2d). In 2016,
163 the lake volume had increased to 17.40 million m³ due to continued deglaciation (ANA, 2016). The potential of fur-
164 ther growth is limited since, as of 2017, Lake Palcacocha is only connected to a small regenerating glacier. Further, the
165 lake level is lowered artificially, using a set of siphons (it decreased by 3 m between December 2016 and July 2017).
166 Table 1 summarizes the major characteristics of Lake Palcacocha in 2016. The overall situation in July 2017 is illustrat-
167 ed in Fig. 2c.

168 2.4 Previous simulations of possible future GLOF process chains

169 Due to its history, recent growth, and catchment characteristics, Lake Palcacocha is considered hazardous for the
170 downstream communities, including the city of Huaráz (Fig. 2e). Whilst Vilímek et al (2005) point out that the lake
171 volume would not allow an event comparable to 1941, by 2016 the lake volume had become much larger than the
172 volume before 1941 (ANA, 2016). Even though the lower potential of dam erosion (Somos-Valenzuela et al., 2016) and
173 the non-existence of Lake Jircacocha make a 1941-magnitude event appear unlikely, the steep glacierized mountain
174 walls in the back of the lake may produce ice or rock-ice avalanches leading to impact waves, dam overtopping, ero-
175 sion, and subsequent mass flows. Investigations by Klimeš et al. (2016) of the steep lateral moraines surrounding the
176 lake indicate that failures and slides from moraines are possible at several sites, but do not have the potential to create
177 a major overtopping wave, partly due to the elongated shape of the lake. Rivas et al. (2015) elaborated on the possible
178 effects of moraine-failure induced impact waves. Recently, Somos-Valenzuela et al. (2016) have used a combination of
179 simulation approaches to assess the possible impact of process chains triggered by ice avalanching into Lake Palcacocha
180 on Huaráz. They considered three scenarios of ice avalanches detaching from the slope of Palcaraju (0.5, 1.0, and
181 3.0 million m³) in order to create flood intensity maps and to indicate travel times of the mass flow to various points of
182 interest. For the large scenario, the mass flow would reach the uppermost part of the city of Huaráz after approx.
183 1 h 20 min, for the other scenarios this time would increase to 2 h 50 min (medium scenario) and 8 h 40 min (small
184 scenario). Particularly for the large scenario, a high level of hazard is identified for a considerable zone near the Quil-
185 cay River, whereas zones of medium or low hazard become more abundant with the medium and small scenarios, or
186 with the assumption of a lowered lake level (Somos-Valenzuela et al., 2016). In addition, Chisolm and McKinney
187 (2018) analyzed the dynamics impulse waves generated by avalanches using FLOW-3D. A similar modelling approach
188 was applied by Frey et al. (2018) to derive a map of GLOF hazard for the Quilcay catchment. For Lake Palcacocha the
189 same ice avalanche scenarios as applied by Somos-Valenzuela et al. (2016) were employed, with correspondingly com-
190 parable results in the Cojup Valley and for the city of Huaráz.

191 3 The r.avaflow computational tool

192 r.avaflow is an open source tool for simulating the dynamics of complex mass flows in mountain areas. It employs a
193 two-phase model including solid particles and viscous fluid, making a difference to most other mass flow simulation
194 tools which build on one-phase mixture models. r.avaflow considers the interactions between the phases as well as
195 erosion and entrainment of material from the basal surface. Consequently, it is well-suited for the simulation of com-

plex, cascading flow-type landslide processes. The r.avaflow framework is introduced in detail by Mergili et al. (2017), only those aspects relevant for the present work are explained here.

The Pudasaini (2012) two-phase flow model is used for propagating mass flows from at least one defined release area through a Digital Terrain Model (DTM). Flow dynamics is computed through depth-averaged equations describing the conservation of mass and momentum for both solid and fluid. The solid stress is computed on the basis of the Mohr-Coulomb plasticity, whereas the fluid is treated with a solid-volume-fraction-gradient-enhanced non-Newtonian viscous stress. Virtual mass due to the relative motion and acceleration, and generalized viscous drag, account for the strong transfer of momentum between the phases. Also buoyancy is considered. The momentum transfer results in simultaneous deformation, separation, and mixing of the phases (Mergili et al., 2018a). Pudasaini (2012) gives a full description of the set of equations.

Certain enhancements are included, compared to the original model: for example, drag and virtual mass are computed according to extended analytical functions constructed by Pudasaini (2019a, b). Additional (complementary) functionalities include surface control, diffusion control, and basal entrainment (Mergili et al., 2017, 2018a, 2019). A conceptual model is used for entrainment: thereby, the empirically derived entrainment coefficient C_E is multiplied with the flow kinetic energy:

$$q_{E,s} = C_E |T_s + T_f| \alpha_{s,E}, \quad q_{E,f} = C_E |T_s + T_f| (1 - \alpha_{s,E}). \quad (1)$$

$q_{E,s}$ and $q_{E,f}$ (m s^{-1}) are the solid and fluid entrainment rates, T_s and T_f (J) are the solid and fluid kinetic energies, and $\alpha_{s,E}$ is the solid fraction of the entrainable material (Mergili et al., 2019). Flow heights and momenta as well as the change of elevation of the basal surface are updated at each time step (Mergili et al., 2017).

Any desired combination of solid and fluid release and entrainable heights can be defined. The main results are raster maps of the evolution of solid and fluid flow heights, velocities, and entrained heights in time. Pressures and kinetic energies are derived from the flow heights and velocities. Output hydrographs can be generated as an additional option (Mergili et al., 2018a). Spatial discretization works on the basis of GIS raster cells: the flow propagates between neighbouring cells during each time step. The Total Variation Diminishing Non-Oscillatory Central Differencing (TVD-NOC) Scheme (Nessyahu and Tadmor, 1990; Tai et al., 2002; Wang et al., 2004) is employed for solving the model equations. This approach builds on a staggered grid, in which the system is shifted half the cell size during each step in time (Mergili et al., 2018b).

r.avaflow operates as a raster module of the open source software GRASS GIS 7 (GRASS Development Team, 2019), employing the programming languages Python and C as well as the R software (R Core Team, 2019). More details about r.avaflow are provided by Mergili et al. (2017).

4 Simulation input

The simulations build on the topography, represented by a DTM, and on particular sets of initial conditions and model parameters. For the DTM, we use a 5 m resolution Digital Elevation Model provided by the Peruvian Ministry of Environment, MINAM (Horizons, 2013). It was deduced from recent stereo aerial photographs and airborne LiDAR. The DEM is processed in order to derive a DTM representing the situation before the 1941 event. Thereby, we neglect the possible error introduced by the effects of vegetation or buildings, and focus on the effects of the lakes and of erosion (Fig. 4):

1. For the area of Lake Palcacocha the elevation of the lake surface is replaced by a DTM of the lake bathymetry derived from ANA (2016). Possible sedimentation since that time is neglected. The photograph of Hans Kinzl

from 1939 (Fig. 2a) is used to reconstruct the moraine dam before the breach, and the glacier at the same time. As an exact positioning of the glacier terminus is not possible purely based on the photo, the position is optimized towards a lake volume of approx. 13 million m³, following the estimate of ANA. It is further assumed that there was surficial drainage of Lake Palcacocha as suggested by Fig. 2a, i.e. the lowest part of the moraine crest is set equal to the former lake level of 4,610 m a.s.l (Fig. 4b).

2. Also for Lake Jircacocha, surficial overflow is assumed (a situation that is observed for most of the recent landslide-dammed lakes in the Cordillera Blanca). On this basis the landslide dam before its breach is reconstructed, guided by topographic and geometric considerations. The lowest point of the dam crest is set to 4,130 m a.s.l. (Fig. 4c).
3. Erosional features along the flow channel are assumed to largely relate to the 1941 event. These features are filled accordingly (see Table 2 for the filled volumes). In particular, the flow channel in the lower part of the valley, reportedly deepened by up to 50 m in the 1941 event (Vilímek et al., 2005), was filled in order to represent the situation before the event in a plausible way (Fig. 4d).

All lakes are considered as fluid release volumes in ravaflow. The initial level of Lake Palcacocha in 1941 is set to 4,610 m a.s.l., whereas the level of Lake Jircacocha is set to 4,129 m a.s.l. The frontal part of the moraine dam impounding Lake Palcacocha and the landslide dam impounding Lake Jircacocha are considered as entrainable volumes. Further, those areas filled up along the flow path (Fig. 4d) are considered entrainable, mainly following Vilímek et al. (2005). However, as it is assumed that part of the material was removed through secondary processes or afterwards, only 75% of the added material are allowed to be entrained. All entrained material is considered 80% solid and 20% fluid per volume.

The reconstructed lake, breach, and entrainable volumes are shown in Tables 1 and 2. The glacier terminus in 1941 was located in an area where the lake depth increases by several tens of metres, so that small misestimates in the position of the glacier tongue may result in large misestimates of the volume, so that some uncertainty has to be accepted.

As the trigger of the sudden drainage of Lake Palcacocha is not clear, we consider four scenarios, based on the situation before the event as shown in the photo taken by Hans Kinzl, experiences from other documented GLOF events in the Cordillera Blanca (Schneider et al., 2014; Mergili et al., 2018a), considerations by Vilímek et al. (2005), Portocarreiro (2014), and Somos-Valenzuela et al. (2016), as well as geotechnical considerations:

- A Retrogressive erosion, possibly induced by minor or moderate overtopping. This scenario is related to a possible minor impact wave, caused for example by calving of ice from the glacier front, an increased lake level due to meteorological reasons, or a combination of these factors. In the simulation, the process chain is started by cutting an initial breach into the dam in order to initiate overtopping and erosion. The fluid phase is considered as pure water.
- AX Similar to Scenario A, but with the second phase considered a mixture of fine mud and water. For this purpose, density is increased to 1,100 instead of 1,000 kg m⁻³, and a yield strength of 5 Pa is introduced (Domnik et al., 2013; Pudasaini and Mergili, 2019; Table 3). For simplicity, we still refer to this mixture as a fluid. Such changed phase characteristics may be related to the input of fine sediment into the lake water (e.g. caused by a landslide from the lateral moraine as triggering event), but are mainly considered here in order to highlight the effects of uncertainties in the definition and parameterization of the two-phase mixture flow.
- B Retrogressive erosion, induced by violent overtopping. This scenario is related to a large impact wave caused by a major rock/ice avalanche or ice avalanche rushing into the lake. In the simulation, the process chain is initiated through a hypothetical landslide of 3 million m³ of 75% solid and 25% fluid material, following the

276 large scenario of Somos-Valenzuela et al. (2016) in terms of volume and release area. In order to be consistent
277 with Scenario A, fluid is considered as pure water.

278 C Internal erosion-induced failure of the moraine dam. Here, the process chain is induced by the collapse of
279 the entire reconstructed breach volume (Fig. 4b). In the simulation, this is done by considering this part of
280 the moraine not as entrainable volume, but as release volume (80% solid, 20% fluid, whereby fluid is again
281 considered as pure water).

282 Failure of the dam of Lake Jircacocha is assumed having occurred through overtopping and retrogressive erosion, in-
283 duced by the increased lake level and a minor impact wave from the flood upstream. No further assumptions of the
284 initial conditions are required in this case.

285 The model parameter values are selected in accordance with experiences gained from previous simulations with
286 r.avaflow for other study areas, and are summarized in Table 3. Three parameters mainly characterizing the flow fric-
287 tion (basal friction of solid δ , ambient drag coefficient C_{AD} , and fluid friction coefficient C_{FF}) and the entrainment coef-
288 ficient C_E are optimized in a spatially differentiated way to maximize the empirical adequacy of the simulations in
289 terms of estimates of impact areas, erosion depths, and flow and breach volumes. As no travel times or velocities are
290 documented for the 1941 event, we use the values given by Somos-Valenzuela et al. (2016) as a rough reference. Vary-
291 ing those four parameters while keeping the others constant helps us to capture variability while minimizing the de-
292 grees of freedom, remaining aware of possible equifinality issues (Beven, 1996; Beven and Freer, 2001).

293 A particularly uncertain parameter is the empirical entrainment coefficient C_E (Eq. 1). In order to optimize C_E , we
294 consider (i) successful prediction of the reconstructed breach volumes; and (ii) correspondence of peak discharge with
295 published empirical equations on the relation between peak discharge, and lake volume and dam height (Walder and
296 O'Connor, 1997). Table 4 summarizes these equations for moraine dams (applied to Lake Palcacocha) and landslide
297 dams (applied to Lake Jircacocha), and the values obtained for the regression and the envelope, using the volumes of
298 both lakes. We note that Table 4 reveals very large differences – roughly one order of magnitude – between regression
299 and envelope. In case of the breach of the moraine dam of Lake Palcacocha, we consider an extreme event due to the
300 steep, poorly consolidated, and maybe soaked moraine, with a peak discharge close to the envelope (approx..
301 $15,000 \text{ m}^3 \text{ s}^{-1}$). For Lake Jircacocha, in contrast, the envelope values of peak discharge do not appear realistic. However,
302 due to the high rate of water inflow from above, a value well above the regression line still appears plausible, even
303 though the usefulness of the empirical laws for this type of lake drainage can be questioned. The value of C_E optimized
304 for the dam of Lake Jircacocha is also used for entrainment along the flow path.

305 All of the computational experiments are run with 10 m spatial resolution. Only flow heights ≥ 25 cm are considered
306 for visualization and evaluation. We now describe one representative simulation result for each of the considered sce-
307 narios, thereby spanning the most plausible and empirically adequate field of simulations.

308 5 r.avaflow simulation results

309 5.1 Scenario A – Event induced by overtopping; fluid without yield strength

310 Outflow from Lake Palcacocha starts immediately, leading to (1) lowering of the lake level and (2) retrogressive ero-
311 sion of the moraine dam. The bell-shaped fluid discharge curve at the hydrograph profile O1 (Fig. 4) reaches its peak
312 of $18,700 \text{ m}^3 \text{ s}^{-1}$ after approx. 780 s, and then decreases to a small residual (Fig. 5a). Channel incision happens quickly –
313 53 m of lowering of the terrain at the reference point R1 occurs in the first less than 1200 s, whereas the lowering at
314 the end of the simulation is 60 m (Fig. 6a). This number represents an underestimation, compared to the reference

315 value of 76 m (Table 2). The lake level decreases by 42 m, whereby 36.5 m of the decrease occur within the first
316 1200 s. The slight underestimation, compared to the reference value of 47 m of lake level decrease, is most likely a
317 consequence of uncertainties in the topographic reconstruction. A total amount of 1.5 million m³ is eroded from the
318 moraine dam of Lake Palcacocha, corresponding to an underestimation of 22%, compared to the reconstructed breach
319 volume. Underestimations mainly occur at both sides of the lateral parts of the eroded channel near the moraine crest
320 – an area where additional post-event erosion can be expected, so that the patterns and degree of underestimation
321 appear plausible (Fig. 7a). In contrast, some overestimation of erosion occurs in the inner part of the dam. For numerical
322 reasons, some minor erosion is also simulated away from the eroded channel. The iterative optimization procedure
323 results in an entrainment coefficient $C_E = 10^{-6.75}$.

324 The deposit of much of the solid material eroded from the moraine dam directly downstream from Lake Palcacocha, as
325 observed in the field (Fig. 2c), is reasonably well reproduced by this simulation, so that the flow proceeding down-
326 valley is dominated by the fluid phase (Fig. 8). It reaches Lake Jircacocha after $t = 840$ s (Fig. 5b). As the inflow occurs
327 smoothly, there is no impact wave in the strict sense, but it is rather the steadily rising water level (see Fig. 6b for the
328 evolution of the water level at the reference point R2) inducing overtopping and erosion of the dam. This only starts
329 gradually after some lag time, at approx. $t = 1,200$ s. The discharge curve at the profile O2 (Fig. 4) reaches its pro-
330 nounced peak of 750 m³ s⁻¹ solid and 14,700 m³ s⁻¹ fluid material at $t = 2,340$ s, and then tails off slowly.

331 In the case of Lake Jircacocha, the simulated breach is clearly shifted south, compared to the observed breach. With
332 the optimized value of the entrainment coefficient $C_E = 10^{-7.15}$, the breach volume is underestimated by 24%, compared
333 to the reconstruction (Fig. 7b). Also here, this intentionally introduced discrepancy accounts for some post-event ero-
334 sion. However, we note that volumes are uncertain as the reconstruction of the dam of Lake Jircacocha – in contrast to
335 Lake Palcacocha – is a rough estimation due to lacking reference data.

336 Due to erosion of the dam of Lake Jircacocha, and also erosion of the valley bottom and slopes, the solid fraction of the
337 flow increases considerably downstream. Much of the solid material, however, is deposited in the lateral parts of the
338 flow channel, so that the flow arriving at Huaráz is fluid-dominated again (Fig. 8). The front enters the alluvial fan of
339 Huaráz at $t = 2,760$ s, whereas the broad peak of 10,500 m³ s⁻¹ of fluid and 2,000 m³ s⁻¹ of solid material (solid fraction
340 of 16%) is reached in the period between 3,600 and 3,780 s (Fig. 4; Fig. 5c). Discharge decreases steadily afterwards. A
341 total of 2.5 million m³ of solid and 14.0 million m³ of fluid material pass the hydrograph profile O3 until $t = 5,400$ s.
342 Referring only to the solid, this is less material than reported by Kaser and Georges (2003). However, (i) there is still
343 some material coming after, and (ii) pore volume has to be added to the solid volume, so that the order of magnitude
344 of material delivered to Huaráz corresponds to the documentation in a better way. Still, the solid ratio of the hydro-
345 graph might represent an underestimation.

346 As prescribed by the parameter optimization, the volumes entrained along the channel are in the same order of mag-
347 nitude, but lower than the reconstructed volumes summarized in Table 2: 0.7 million m³ of material are entrained
348 upstream and 1.5 million m³ downstream of Lake Jircacocha, and 5.3 million m³ in the promontory. Fig. 9a summariz-
349 es the travel times and the flow velocities of the entire process chain. Frontal velocities mostly vary between 5 m s⁻¹
350 and 20 m s⁻¹, with the higher values in the steeper part below Lake Jircacocha. The low and undefined velocities di-
351 rectly downstream of Lake Jircacocha reflect the time lag of substantial overtopping. The key numbers in terms of
352 times, discharges, and volumes are summarized in Table 5.

353 5.2 Scenario AX – Event induced by overtopping; fluid with yield strength

354 Adding a yield strength of $\tau_y = 5$ Pa to the characteristics of the fluid substantially changes the temporal rather than
355 the spatial evolution of the process cascade. As the fluid now behaves as fine mud instead of water and is more re-

356 sistant to motion, velocities are lower, travel times are much longer, and the entrained volumes are smaller than in the
357 Scenario A (Fig. 9b; Table 5). The peak discharge at the outlet of Lake Palcacocha is reached at $t = 1,800$ s. Fluid peak
358 discharge of $8,200 \text{ m}^3 \text{ s}^{-1}$ is less than half the value yielded in Scenario A (Fig. 5d). The volume of material eroded from
359 the dam is only slightly smaller than in Scenario A (1.4 versus 1.5 million m^3). The numerically induced false positives
360 with regard to erosion observed in Scenario A are not observed in Scenario AX, as the resistance to oscillations in the
361 lake is higher with the added yield strength (Fig. 7c). Still, the major patterns of erosion and entrainment are the same.
362 Interestingly, erosion is deeper in Scenario AX, reaching 76 m at the end of the simulation (Fig. 6c) and therefore the
363 base of the entrainable material (Table 2). This is most likely a consequence of the spatially more concentrated flow
364 and therefore higher erosion rates along the centre of the breach channel, with less lateral spreading than in Scenar-
365 io A.

366 Consequently, also Lake Jircacocha is reached later than in Scenario A (Fig. 6d), and the peak discharge at its outlet is
367 delayed ($t = 4,320$ s) and lower ($7,600 \text{ m}^3 \text{ s}^{-1}$ of fluid and $320 \text{ m}^3 \text{ s}^{-1}$ of solid material) (Fig. 5e). 2.0 million m^3 of materi-
368 al are entrained from the dam of Lake Jircacocha, with similar spatial patterns as in Scenario A (Fig. 7d). Huaráz is
369 reached after $t = 4,200$ s, and the peak discharge of $5,000 \text{ m}^3 \text{ s}^{-1}$ of fluid and $640 \text{ m}^3 \text{ s}^{-1}$ of solid material at O3 occurs
370 after $t = 6,480$ s (Fig. 5f). This corresponds to a solid ratio of 11%. Interpretation of the solid ratio requires care here as
371 the fluid is defined as fine mud, so that the water content is much lower than the remaining 89%. The volumes en-
372 trained along the flow channel are similar in magnitude to those obtained in the simulation of Scenario A (Table 5).

373 5.3 Scenario B – Event induced by impact wave

374 Scenario B is based on the assumption of an impact wave from a 3 million m^3 landslide. However, due to the relatively
375 gently-sloped glacier tongue heading into Lake Palcacocha at the time of the 1941 event (Figs. 2a and 4b), only a small
376 fraction of the initial landslide volume reaches the lake, and impact velocities and energies are reduced, compared to a
377 direct impact from the steep slope. Approx. 1 million m^3 of the landslide have entered the lake until $t = 120$ s, an
378 amount which only slightly increases thereafter. Most of the landslide deposits on the glacier surface. Caused by the
379 impact wave, discharge at the outlet of Lake Palcacocha (O1) sets on at $t = 95$ s and, due to overtopping of the impact
380 wave, immediately reaches a relatively moderate first peak of $7,000 \text{ m}^3 \text{ s}^{-1}$ of fluid discharge. The main peak of
381 $16,900 \text{ m}^3 \text{ s}^{-1}$ of fluid and $2,000 \text{ m}^3 \text{ s}^{-1}$ of solid discharge occurs at $t = 1,200$ s due do the erosion of the breach channel.
382 Afterwards, discharge decreases relatively quickly to a low base level (Fig. 10a). The optimized value of $C_E = 10^{-6.75}$ is
383 used also for this scenario. The depth of erosion along the main path of the breach channel is clearly less than in the
384 Scenario A (Fig. 6e). However, Table 5 shows a higher volume of eroded dam material than the other scenarios. These
385 two contradicting patterns are explained by Fig. 11a: the overtopping due to the impact wave does not only initiate
386 erosion of the main breach, but also of a secondary breach farther north. Consequently, discharge is split among the
387 two breaches and therefore less concentrated, explaining the lower erosion at the main channel despite a larger total
388 amount of eroded material. The secondary drainage channel can also be deduced from observations (Fig. 3a), but has
389 probably played a less important role than suggested by this simulation.

390 The downstream results of Scenario B largely correspond to the results of the Scenario A, with some delay partly relat-
391 ed to the time from the initial landslide to the overtopping of the impact wave. Discharge at the outlet of Lake Jircaco-
392 cha peaks at $t = 2,700$ s (Fig. 10b), and the alluvial fan of Huaráz is reached after 3,060 s (Fig. 10c). The peak discharges
393 at O2 and O3 are similar to those obtained in the Scenario A. The erosion patterns at the dam of Lake Jircacocha
394 (again, $C_E = 10^{-7.15}$) very much resemble those yielded with the scenarios A and AX (Fig. 11b), and so does the volume
395 of entrained dam material (2.2 million m^3). The same is true for the 2.5 million m^3 of solid and 13.9 million m^3 of fluid
396 material entering the area of Huaráz until $t = 5,400$ s, according to this simulation.

397 Also in this scenario, the volumes entrained along the flow channel are very similar to those obtained in the simula-
398 tion of Scenario A. The travel times and frontal velocities – resembling the patterns obtained in Scenario A, with the
399 exception of the delay – are shown in Fig. 12a, whereas Table 5 summarizes the key numbers in terms of times, vol-
400 umes, and discharges.

401 5.4 Scenario C – Event induced by dam collapse

402 In Scenario C, we assume that the breached part of the moraine dam collapses, the collapsed mass mixes with the wa-
403 ter from the suddenly draining lake, and flows downstream. The more sudden and powerful release, compared to the
404 two other scenarios, leads to higher frontal velocities and shorter travel times (Fig. 12b; Table 5).

405 In contrast to the other scenarios, impact downstream starts earlier, as more material is released at once, instead of
406 steadily increasing retrogressive erosion and lowering of the lake level. The fluid discharge at O1 peaks at almost
407 $40,000 \text{ m}^3 \text{ s}^{-1}$ (Fig. 10d) rapidly after release. Consequently, Lake Jircacocha is reached already after 720 s, and the im-
408 pact wave in the lake evolves more quickly than in all the other scenarios considered (Fig. 6f). The lake drains with a
409 peak discharge of $15,400 \text{ m}^3 \text{ s}^{-1}$ of fluid and $830 \text{ m}^3 \text{ s}^{-1}$ of solid material after 1,680–1,740 s (Fig. 10e). In contrast to the
410 more rapid evolution of the process chain, discharge magnitudes are largely comparable to those obtained with the
411 other scenarios. The same is true for the hydrograph profile O3: the flow reaches the alluvial fan of Huaráz after
412 $t = 2,160 \text{ s}$, with a peak discharge slightly exceeding $10,000 \text{ m}^3 \text{ s}^{-1}$ of fluid and $2,000 \text{ m}^3 \text{ s}^{-1}$ of solid material between
413 $t = 2,940 \text{ s}$ and $3,240 \text{ s}$. 2.7 million m^3 of solid and 14.6 million m^3 of fluid material enter the area of Huaráz until
414 $t = 5,400 \text{ s}$, which is slightly more than in the other scenarios, indicating the more powerful dynamics of the flow (Ta-
415 ble 5). The fraction of solid material arriving at Huaráz remains low, with 16% solid at peak discharge and 15% in to-
416 tal. Again, the volumes entrained along the flow channel are very similar to those obtained with the simulations of the
417 other scenarios (Table 5).

418 6 Discussion

419 6.1 Possible trigger of the GLOF process chain

420 In contrast to other GLOF process chains in the Cordillera Blanca, such as the 2010 event at Laguna 513 (Schneider et
421 al., 2014), which was clearly triggered by an ice-rock avalanche into the lake, there is disagreement upon the trigger of
422 the 1941 multi-lake outburst flood in the Quilcay catchment. Whereas, according to contemporary reports, there is no
423 evidence of a landslide (for example, ice avalanche) impact onto the lake (Vilímek et al., 2005; Wegner, 2014), and
424 dam rupture would have been triggered by internal erosion, some authors postulate an at least small impact starting
425 the process chain (Portocarrero, 2014; Somos-Valenzuela et al., 2016).

426 Each of the three assumed initiation mechanisms of the 1941 event, represented by the Scenarios A/AX, B, and C,
427 yields results which are plausible in principle. We consider a combination of all three mechanisms a likely cause of
428 this extreme process chain. Overtopping of the moraine dam, possibly related to a minor impact wave, leads to the
429 best correspondence of the model results with the observation, documentation, and reconstruction. Particularly the
430 signs of minor erosion of the moraine dam north of the main breach (Fig. 3a) support this conclusion: a major impact
431 wave, resulting in violent overtopping of the entire frontal part of the moraine dam, would supposedly also have led to
432 more pronounced erosion in that area, as to some extent predicted by the Scenario B. There is also no evidence for
433 strong landslide-glacier interactions (massive entrainment of ice or even detachment of the glacier tongue) which
434 would be likely scenarios in the case of a very large landslide. Anyway, the observations do not allow for substantial
435 conclusions on the volume of a hypothetical triggering landslide: as suggested by Scenario B, even a large landslide from

436 the slopes of Palcaraju or Pucaranra could have been partly alleviated on the rather gently sloped glacier tongue be-
437 tween the likely release area and Lake Palcacocha.

438 The minor erosional feature north of the main breach was already visible in the photo of Kinzl (Fig. 2a), possibly indi-
439 cating an earlier, small GLOF. It remains unclear whether it was reactivated in 1941. Such a reactivation could only be
440 directly explained by an impact wave, but not by retrogressive erosion only (A/AX) or internal failure of the dam (C) –
441 so, more research is needed here. The source area of a possible impacting landslide could have been the slopes of Pal-
442 caraju or Pucaranra (Fig. 1), or the calving glacier front (Fig. 2a). Attempts to quantify the most likely release volume
443 and material composition would be considered speculative due to the remaining difficulties in adequately simulating
444 landslide-(glacier-)lake interactions (Westoby et al., 2014). Further research is necessary in this direction. In any case,
445 a poor stability condition of the dam (factor of safety ~ 1) could have facilitated the major retrogressive erosion of the
446 main breach. A better understanding of the hydro-mechanical load applied by a possible overtopping wave and the
447 mechanical strength of the moraine dam could help to resolve this issue.

448 The downstream patterns of the flow are largely similar for each of the scenarios A, AX, B, and C, with the exception
449 of travel times and velocities. Interaction with Lake Jircacocha disguises much of the signal of process initiation. Lag
450 times between the impact of the flow front on Lake Jircacocha and the onset of substantial overtopping and erosion
451 are approx. 10 minutes in the scenarios A and B, and less than 3 minutes in the Scenario C. This clearly reflects the
452 slow and steady onset of those flows generated through retrogressive erosion. The moderate initial overtopping in
453 Scenario B seems to alleviate before reaching Lake Jircacocha. Sudden mechanical failure of the dam (Scenario C), in
454 contrast, leads to a more sudden evolution of the flow, with more immediate downstream consequences.

455 6.2 Parameter uncertainties

456 We have tried to back-calculate the 1941 event in a way reasonably corresponding to the observation, documentation
457 and reconstruction, and building on physically plausible parameter sets. Earlier work on the Huascarán landslides of
458 1962 and 1970 has demonstrated that empirically adequate back-calculations are not necessarily plausible with regard
459 to parameterization (Mergili et al., 2018b). This issue may be connected to equifinality issues (Beven, 1996; Beven and
460 Freer, 2001), and in the case of the very extreme and complex Huascarán 1970 event, by the inability of the flow mod-
461 el and its numerical solution to adequately reproduce some of the process components (Mergili et al., 2018b). In the
462 present work, however, reasonable levels of empirical adequacy and physical plausibility are achieved. Open questions
463 remain with regard to the spatial differentiation of the basal friction angle required to obtain adequate results (Ta-
464 ble 3): lower values of δ downstream from the dam of Lake Jircacocha are necessary to ensure that a certain fraction of
465 solid passes the hydrograph profile O3 and reaches Huaráz. Still, solid fractions at O3 appear rather low in all simula-
466 tions. A better understanding of the interplay between friction, drag, virtual mass, entrainment, deposition, and phase
467 separation could help to resolve this issue (Pudasaini and Fischer, 2016a, b; Pudasaini, 2019a, b).

468 The empirically adequate reproduction of the documented spatial patterns is only one part of the story (Mergili et al.,
469 2018a). The dynamic flow characteristics (velocities, travel times, hydrographs) are commonly much less well docu-
470 mented, particularly for events in remote areas which happened a long time ago. Therefore, direct references for eval-
471 uating the empirical adequacy of the dimension of time in the simulation results are lacking. However, travel times
472 play a crucial role related to the planning and design of (early) warning systems and risk reduction measures (Hof-
473 flinger et al., 2019). Comparison of the results of the scenarios A and AX (Fig. 9) reveals almost doubling travel times
474 when adding a yield stress to the fluid fraction. In both scenarios, the travel times to Huaráz are within the same order
475 of magnitude as the travel times simulated by Somos-Valenzuela et al. (2016) and therefore considered plausible, so
476 that it is hard to decide about the more adequate assumption. Even though the strategy of using the results of earlier

477 simulations as reference may increase the robustness of model results, it might also reproduce errors and inaccuracies
478 of earlier simulation attempts, and thereby confirm wrong results.

479 The large amount of more or less pure lake water would point towards the Scenario A, whereas intense mixing and
480 entrainment of fine material would favour the Scenario AX. More work is necessary in this direction, also considering
481 possible phase transformations (Pudasaini and Krautblatter, 2014). At the same time, the optimization and evaluation
482 of the simulated discharges remains a challenge. Here we rely on empirical relationships gained from the analysis of
483 comparable events (Walder and O'Connor, 1997).

484 6.3 Implications for predictive simulations

485 Considering what was said above, the findings from the back-calculation of the 1941 event can help us to better un-
486 derstand and constrain possible mechanisms of this extreme process chain. In principle, such an understanding can be
487 transferred to present hazardous situations in order to inform the design of technical remediation measures. Earlier,
488 measures were not only implemented at Lake Palcacocha (Portocarrero, 2014), but also at various other lakes such as
489 Laguna 513: a tunnelling scheme implemented in the 1990s strongly reduced the impacts of the 2010 GLOF process
490 chain (Reynolds, 1998; Reynolds et al., 1998; Schneider et al., 2014).

491 However, the findings of this study should only be applied for forward simulations in the same area or other areas
492 with utmost care. The initial conditions and model parameters are not necessarily valid for events of different charac-
493 teristics and magnitudes (Mergili et al., 2018b). In the case of Lake Palcacocha, the situation has changed substantially
494 since 1941: the lake level is much lower and the volume larger, and the lake is directly connected to the steep glacier-
495 ized slopes, so that the impact of a hypothetical landslide could be very different now. Also, the current lake is dammed
496 by another moraine than the pre-1941 lake, with a very different dam geometry (Somos-Valenzuela et al., 2016). In
497 general, the mechanisms of the landslide impact into the lake, which were not the focus of the present study, would
498 require more detailed investigations. Ideally, such work would be based on a three-phase model (Pudasaini and
499 Mergili, 2019; considering ice as a separate phase), and consider knowledge and experience gained from comparable,
500 well-documented events. A possible candidate for such an event would be the 2010 event at Laguna 513, which was
501 back-calculated by Schneider et al. (2014). In general, it remains a challenge to reliably predict the outcomes of given
502 future scenarios. The magnitude of the 1941 event was amplified by the interaction with Lake Jircacocha, whereas the
503 2012 GLOF process chain in the Santa Cruz Valley (Mergili et al., 2018a) alleviated due to the interaction with Lake
504 Jatuncocha, comparable in size. While it seems clear that the result of such an interaction depends on event magni-
505 tude, topography, and the dam characteristics of the impacted lake, Mergili et al. (2018a, b) have demonstrated the
506 high sensitivity of the behaviour of the simulated flow to the friction parameters, but also to the material involved
507 (release mass, entrainment). A larger number of back-calculated process chains will be necessary to derive guiding
508 parameter sets which could facilitate predictive simulations, and so will an appropriate consideration of model uncer-
509 tainties and possible threshold effects (Mergili et al., 2018b). Earlier studies, considering the 2010 event at Laguna 513
510 (Schneider et al., 2014) and three future scenarios for Lake Palcacocha (Somos-Valenzuela et al., 2016) have followed a
511 different strategy, using model cascades instead on integrated simulations, so that a comparison with studies based on
512 r.avaflow is only possible to a limited extent.

513 Another remaining issue is the lateral spreading of the flow on the fan of Huaráz, which is overestimated in all four
514 simulations (Figs. 8, 9, and 12): the most likely reason for this is the insufficient representation of fine-scale structures
515 such as buildings or walls in the DEM, which would serve as obstacles confining the flow in lateral direction.

7 Conclusions

We have performed back-calculations of the documented 1941 GLOF process chain involving Lake Palcacocha and Lake Jircacocha in the Quilcay catchment in the Cordillera Blanca, Perú. The key messages of this work are summarized as follows:

- Retrogressive erosion, possibly caused by a minor impact wave, appears to be the most likely release mechanism of the process chain, facilitated by a geotechnically poorly stable dam with a low width-to-height ratio. This type of failure – a combination of the idealized scenarios considered in this work – can be inferred from observations, and appears most plausible with regard to the simulation results. The identification of the triggering process remains difficult, also because the subsequent interaction with Lake Jircacocha disguises part of the respective signature downstream.
- The correspondence between simulation results and observations is reasonable, and the model parameter values used are physically plausible. However, considerable uncertainties remain with regard to peaks and shapes of the discharge hydrographs, and to the quantification of flow velocities and travel times. Adding a yield strength to the fluid phase (Scenario AX) completely changes the temporal, but not the spatial evolution of the flow. Still, travel times remain in the same order of magnitude as those derived by Somos-Valenzuela et al. (2016) for possible future events.
- Transfer of the findings to forward simulations in the same area or elsewhere remains a challenge due to differences in the initial conditions, uncertainties of the reference data, equifinality issues, and the effects of process magnitude (Mergili et al., 2018b).

Code availability

The model codes of `r.avaflow`, a manual, training data, and the necessary start scripts can be obtained from [Mergili and Pudasaini \(2019\)](#).

Data availability

The original DEM was provided by MINAM and may not be freely distributed, but all data derived within the present work can be obtained by directly contacting the first author (martin.mergili@boku.ac.at).

Author contribution

MM developed the main ideas, defined the scenarios, did most of the data processing, simulations, and analyses, wrote the major portion of the text, and prepared all the figures and tables. SP provided important ideas with regard to the numerical simulations and contributed to the internal revision and optimization of the manuscript. AE contributed with important ideas, conducted field work, acquired data, contributed to the writing of the introductory chapters, and took part in the internal revision and optimization of the manuscript. JTF provided important contributions to the internal revision and optimization of the work. AC provided important data and contributed to the internal revision and optimization of the manuscript. HF contributed with important ideas and field work, data acquisition, and text blocks for the introductory chapters, and took part in the internal revision and optimization of the manuscript.

550 **Competing interests**

551 The authors declare that they have no conflict of interest.

552 **Acknowledgements**

553 Part of this work was conducted within the international cooperation project “A GIS simulation model for avalanche
554 and debris flows (avaflow)” supported by the German Research Foundation (DFG, project number PU 386/3-1) and
555 the Austrian Science Fund (FWF, project number I 1600-N30). Shiva P. Pudasaini further acknowledges financial sup-
556 port from DFG through the research project “A novel and unified solution to multi-phase mass flows: U_MultiSol”.
557 The work also follows the AKTION Austria – Czech Republic project “Currently forming glacial lakes: potentially
558 hazardous entities in deglaciating high mountains” of Adam Emmer and Martin Mergili. Further, the support provided
559 by the Swiss Agency for Development and Cooperation (SDC) through Proyecto Glaciares+, is acknowledged. Adam
560 Emmer was also supported by the Ministry of Education, Youth and Sports of the Czech Republic within the National
561 Sustainability Programme I (NPU I), grant number LO1415, and the postdoc grant of the Czech Academy of Sciences.
562 Finally, we are grateful to Matthias Benedikt for comprehensive technical support in relation to r.avaflow.

563 **References**

564 ANA: Inventario Nacional de Glaciares y Lagunas – Lagunas, Ministerio de Agricultura y Riesgo, Autoridad Nacional
565 del Agua, Unidad de Glaciología y Recursos Hídricos, Huaráz, Peru, 2014.

566 ANA: Plano batimétrico de la Laguna Palcacocha. Perfil longitudinal y transversal, Ministerio de Agricultura y Riesgo,
567 Autoridad Nacional del Agua, Unidad de Glaciología y Recursos Hídricos, Huaráz, Peru, 2016.

568 Andres, C. N., Eyles, C. H., Jara, H., and Narro-Pérez, R.: Sedimentological analysis of Paleolake Jircacocha, Cojup
569 Valley, Cordillera Blanca, Peru. *Revista de Glaciares y Ecosistemas de Montaña*, 5, 9–26, 2018.

570 Beven, K.: Equifinality and Uncertainty in Geomorphological Modelling, in: *The Scientific Nature of Geomorphology:*
571 *Proceedings of the 27th Binghamton Symposium in Geomorphology*, 27–29 September 1996, John Wiley & Sons, 289–
572 313, 1996.

573 Beven, K., and Freer, J.: Equifinality, data assimilation, and uncertainty estimation in mechanistic modelling of com-
574 plex environmental systems using the GLUE methodology, *J. Hydrol.*, 249(1), 11–29, [https://doi.org/10.1016/S0022-](https://doi.org/10.1016/S0022-1694(01)00421-8)
575 [1694\(01\)00421-8](https://doi.org/10.1016/S0022-1694(01)00421-8), 2001.

576 Bolch, T., Peters, J., Yegorov, A., Prafhan, B., Buchroithner, M., and Blagoveshchensky, V.: Identification of potential-
577 ly dangerous glacial lakes in the northern Tien Shan, *Nat. Hazards*, 59, 1691–1714, [https://doi.org/10.1007/s11069-011-](https://doi.org/10.1007/s11069-011-9860-2)
578 [9860-2](https://doi.org/10.1007/s11069-011-9860-2), 2011.

579 Breien, H., De Blasio, F. V., Elverhoi, A., and Hoeg, K.: Erosion and morphology of a debris flow caused by a glacial
580 lake outburst flood, Western Norway, *Landslides*, 5(3), 271–280, <https://doi.org/10.1007/s10346-008-0118-3>, 2008.

581 Broggi, J. A.: Informe preliminar sobre la exploracion y estudio de las condiciones de estabilidad de las lagunas de la
582 Cordillera Blanca, ELECTROPERU S.A., Lima, Peru, 1942.

583 Carey, M.: Living and dying with glaciers: people's historical vulnerability to avalanches and outburst floods in Peru.
584 *Glob. Planet. Change*, 47, 122–134, <https://doi.org/10.1016/j.gloplacha.2004.10.007>, 2005.

Carey, M., Huggel, C., Bury, J., Portocarrero, C., and Haeberli, W.: An integrated socio-environmental framework for glacier hazard management and climate change adaptation: lessons from Lake 513, Cordillera Blanca, Peru, *Clim. Change*, 112(3), 733–767, <https://doi.org/10.1007/s10584-011-0249-8>, 2012.

Carey, M., McDowell, G., Huggel, C., Jackson, M., Portocarrero, C., Reynolds, J.M., and Vicuña, L.: Integrated approaches to adaptation and disaster risk reduction in dynamic socio-cryospheric systems, in: *Snow and Ice-related Hazards, Risks and Disasters*, edited by: Haeberli, W., and Whiteman, C., 219–261, Elsevier, <https://doi.org/10.1016/B978-0-12-394849-6.00008-1>, 2014.

Chisolm, R. E., and McKinney, D. C.: Dynamics of avalanche-generated impulse waves: three-dimensional hydrodynamic simulations and sensitivity analysis, *Nat. Hazards Earth Syst. Sci.*, 18, 1373–1393, <https://doi.org/10.5194/nhess-18-1373-2018>, 2018.

Christen, M., Kowalski, J., and Bartelt, P.: RAMMS: Numerical simulation of dense snow avalanches in three-dimensional terrain, *Cold Reg. Sci. Technol.*, 63, 1–14, <https://doi.org/10.1016/j.coldregions.2010.04.005>, 2010.

Clague, J. J., and O'Connor, J. E.: Glacier-related outburst floods, in: *Snow and Ice-related Hazards, Risks and Disasters*, edited by: Haeberli, W., and Whiteman, C., 487–519, Elsevier, <https://doi.org/10.1016/B978-0-12-394849-6.00014-7>, 2014.

Concha, J. F.: *Síntesis de los trabajos efectuados por la comisión de las lagunas de la Cordillera Blanca*, Ministerio de Fomento, Comisión de Control de las Lagunas de la Cordillera Blanca (CCLCB), Lima, Peru, 1952.

Domnik, B., Pudasaini, S. P., Katzenbach, R., and Miller, S. A.: Coupling of full two-dimensional and depth-averaged models for granular flows, *J. Non-Newtonian Fluid Mech.*, 201, 56–68, <https://doi.org/10.1016/j.jnnfm.2013.07.005>, 2013.

Emmer, A.: Geomorphologically effective floods from moraine-dammed lakes in the Cordillera Blanca, Peru, *Quat. Sci. Rev.*, 177, 220–234, <https://doi.org/10.1016/j.quascirev.2017.10.028>, 2017.

Emmer, A., and Vilímek, V.: Review Article: Lake and breach hazard assessment for moraine-dammed lakes: an example from the Cordillera Blanca (Peru), *Nat. Hazards Earth Syst. Sci.*, 13, 1551–1565, <https://doi.org/10.5194/nhess-13-1551-2013>, 2013.

Emmer, A., and Vilímek, V.: New method for assessing the susceptibility of glacial lakes to outburst floods in the Cordillera Blanca, Peru, *Hydrol. Earth Syst. Sci.*, 18, 3461–3479, <https://doi.org/10.5194/hess-18-3461-2014>, 2014.

Emmer, A., Klimeš, J., Mergili, M., Vilímek, V., and Cochachin, A.: 882 lakes of the Cordillera Blanca: an inventory, classification and assessment of susceptibility to outburst flood, *Catena*, 147, 269–279, <https://doi.org/10.1016/j.catena.2016.07.032>, 2016.

Emmer, A., Merkl, S., and Mergili, M.: Spatiotemporal patterns of high-mountain lakes and related hazards in western Austria, *Geomorphology*, 246, 602–616, <https://doi.org/10.1016/j.geomorph.2015.06.032>, 2015.

Emmer, A., Vilímek, V., and Zapata, M. L.: Hazard mitigation of glacial lake outburst floods in the Cordillera Blanca (Peru): the effectiveness of remedial works, *J. Flood Risk Manag.*, 11, 489–501, <https://doi.org/10.1111/jfr3.12241>, 2018.

Emmer, A., Harrison, S., Mergili, M., Allen, S., Frey, H., and Huggel, C.: A 70 year record of lake evolution and Glacial Lake Outburst Floods in the Peruvian Andes, *Proc. Natl. Acad. Sci. U. S. A.*, submitted manuscript, 2019.

622 Evans, S. G., Bishop, N.F., Fidel Smoll, L., Valderrama Murillo, P., Delaney, K.B., and Oliver-Smith, A.: A re-
623 examination of the mechanism and human impact of catastrophic mass flows originating on Nevado Huascarán, Cor-
624 dillera Blanca, Peru in 1962 and 1970, *Eng. Geol.*, 108, 96–118, <https://doi.org/10.1016/j.enggeo.2009.06.020>, 2009.

625 Frey, H., Huggel, C., Chisolm, R. E., Baer, P., McArdeell, B., Cochachin, A., and Portocarrero, C.: Multi-Source Glacial
626 Lake Outburst Flood Hazard Assessment and Mapping for Huaráz, Cordillera Blanca, Peru, *Front. Earth Sci.*, 6, 210,
627 <https://doi.org/10.3389/feart.2018.00210>, 2018.

628 Gabl, R., Seibl, J., Gems, B., and Aufleger, M.: 3-D numerical approach to simulate the overtopping volume caused by
629 an impulse wave comparable to avalanche impact in a reservoir, *Nat. Hazards Earth Syst. Sci.*, 15, 2617–2630,
630 <https://doi.org/10.5194/nhess-15-2617-2015>, 2015.

631 GAPHAZ: Assessment of glacier and permafrost hazards in Mountain Regions, in: Joint Standing Group on Glacier and
632 Permafrost Hazards in High Mountains (GAPHAZ) of the International Association of Cryospheric Sciences (IACS)
633 and the International Permafrost Association (IPA), edited by: Allen, S. K., Frey, H., and Huggel, C., Zurich, Lima,
634 available online at: http://gaphaz.org/files/Assessment_Glacier_Permafrost_Hazards_Mountain_Regions.pdf, 2017.

635 GRASS Development Team: Geographic Resources Analysis Support System (GRASS) Software, Open Source Geospa-
636 tial Foundation Project, <https://grass.osgeo.org>, last access: 4 February 2019.

637 Haeberli, W.: Frequency and characteristics of glacier floods in the Swiss Alps, *Ann. Glaciol.*, 4, 85–90,
638 <https://doi.org/10.3189/S0260305500005280>, 1983.

639 Harrison, S., Kargel, J. S., Huggel, C., Reynolds, J., Shugar, D. H., Betts, R. A., Emmer, A., Glasser, N., Haritashya, U.
640 K., Klimeš, J., Reinhardt, L., Schaub, Y., Wilyshire, A., Regmi, D., and Vilímek, V.: Climate change and the global pat-
641 tern of moraine-dammed glacial lake outburst floods. *Cryosphere*, 12, 1195–1209, [https://doi.org/10.5194/tc-12-1195-](https://doi.org/10.5194/tc-12-1195-2018)
642 2018, 2018.

643 Hewitt, K., and Liu, J.: Ice-dammed lakes and outburst floods, Karakoram Himalaya: historical perspectives on emerg-
644 ing threats, *Phys. Geogr.*, 31(6), 528–551, <https://doi.org/10.2747/0272-3646.31.6.528>, 2010.

645 Hewitt, K.: Natural dams and outburst floods in the Karakorum Himalaya, in: *Hydrological aspects of alpine and high-*
646 *mountain areas*, edited by: Glen, J. W., IAHS Publication, 138, 259–269, 1982.

647 Hofflinger, A., Somos-Valenzuela, M.A., and Vallejos-Romero, A.: Response time to flood events using a social vulner-
648 ability index (ReTSVI), *Nat. Hazards Earth Syst. Sci.*, 19, 251–267, <https://doi.org/10.5194/nhess-19-251-2019>, 2019.

649 Horizons: Horizons South America S.A.C.: Informe Técnico del Proyecto, Consultoría Para El Levantamiento Foto-
650 gramétrico Detallado De La Sub Cuenca Del Río Quillcay Y La Ciudad De Huaráz Para El Proyecto, Imple-
651 mentación de Medidas de Adaptación al Cambio Climático y Gestión de Riesgos en la Subcuenca Quillcay (IMACC-
652 QUILLCAY) – BID-MINAM (PE-T1168), Ministerio Del Ambiente A Travel Del Fonam – Administrador De Los Re-
653 cursos Del BID, Lima, Peru, 2013.

654 Hubbard, B., Heald, A., Reynolds, J. M., Quincey, D., Richardson, S.D., Luyo, M.Z., Portilla, N.S., and Hambrey, M.J.:
655 Impact of a rock avalanche on a moraine-dammed proglacial lake: Laguna Safuna Alta, Cordillera Blanca, Peru, *Earth*
656 *Surf. Proc. Landforms*, 30(10), 1251–1264, <https://doi.org/10.1002/esp.1198>, 2005.

657 Huggel, C., Käab, A., Haeberli, W., and Krummenacher, B.: Regional-scale GIS-models for assessment of hazards from
658 glacier lake outbursts: evaluation and application in the Swiss Alps, *Nat. Hazards Earth Syst. Sci.*, 3, 647–662,
659 <https://doi.org/10.5194/nhess-3-647-2003>, 2003.

660 Iturrizaga, L.: Glacial and glacially conditioned lake types in the Cordillera Blanca, Peru: A spatiotemporal conceptual
661 approach, *Prog. Phys. Geogr.*, 38, 602–636, <https://doi.org/10.1177/0309133314546344>, 2014.

662 Iverson, R. M.: The physics of debris flows, *Rev. Geophys.*, 35, 245–296, <https://doi.org/10.1029/97RG00426>, 1997.

663 Kafle, J., Pokhrel, P. R., Khattri, K. B., Kattel, P., Tuladhar, B. M., and Pudasaini, S. P.: Landslide-generated tsunami
664 and particle transport in mountain lakes and reservoirs, *Ann. Glaciol.*, 57(71), 232–244,
665 <https://doi.org/10.3189/2016AoG71A034>, 2016.

666 Kafle, J., Kattel, P., Mergili, M., Fischer, J.-T., and Pudasaini, S. P.: Dynamic response of submarine obstacles to two-
667 phase landslide and tsunami impact on reservoirs. *Acta Mech.*, 230(9), 3143–3169, <https://doi.org/10.1007/s00707-019-02457-0>, 2019.

669 Kaser, G., and Georges, C.: A potential disaster in the Icy Andes: a regrettable blunder, technical report, University of
670 Innsbruck, Austria, 2003.

671 Kattel, P., Khattri, K. B., Pokhrel, P. R., Kafle, J., Tuladhar, B. M., and Pudasaini, S. P.: Simulating glacial lake out-
672 burst floods with a two-phase mass flow model, *Ann. Glaciol.*, 57(71), 349–358,
673 <https://doi.org/10.3189/2016AoG71A039>, 2016.

674 Kinzl, H., and Schneider, E.: Cordillera Blanca (Perú), Universitäts-Verlag Wagner, Innsbruck, Austria, 1950.

675 Klimeš, J., Novotný, J., Novotná, I., de Urries, B. J., Vilímek, V., Emmer, A., Strozzi, T., Kusák, M., Cochachin, A.,
676 Hartvich, F., and Frey, H.: Landslides in moraines as triggers of glacial lake outburst floods: example from Palcacocha
677 Lake (Cordillera Blanca, Peru), *Landslides*, 13(6), 1461–1477, <https://doi.org/10.1007/s10346-016-0724-4>, 2016.

678 McDougall, S., and Hungr, O.: A Model for the Analysis of Rapid Landslide Motion across Three-Dimensional Terrain,
679 *Can. Geotech. J.*, 41, 1084–1097, <https://doi.org/10.1139/t04-052>, 2004.

680 Mergili, M., and Pudasaini, S. P.: r.avaflow – The open source mass flow simulation model, <https://www.avaflow.org/>,
681 last access: 9 July 2019.

682 Mergili, M., and Schneider, J. F.: Regional-scale analysis of lake outburst hazards in the southwestern Pamir, Tajiki-
683 stan, based on remote sensing and GIS, *Nat. Hazards Earth Syst. Sci.*, 11, 1447–1462, <https://doi.org/10.5194/nhess-11-1447-2011>, 2011.

685 Mergili, M., Schneider, D., Worni, R., and Schneider, J.F.: Glacial Lake Outburst Floods (GLOFs): challenges in predic-
686 tion and modelling, in: Proceedings of the 5th International Conference on Debris-Flow Hazards Mitigation: Mechan-
687 ics, Prediction and Assessment, Padova, June 14–17, 2011, edited by: Genevois, R., Hamilton, D. L., and Prestininzi,
688 A., *Italian Journal of Engineering Geology and Environment – Book*, 973–982, 2011.

689 Mergili, M., Müller, J. P., and Schneider, J. F.: Spatio-temporal development of high-mountain lakes in the headwaters
690 of the Amu Darya river (Central Asia), *Glob. Planet. Change*, 107, 13–24,
691 <https://doi.org/10.1016/j.gloplacha.2013.04.001>, 2013.

692 Mergili, M., Fischer, J.-T., Krenn, J., and Pudasaini, S. P.: r.avaflow v1, an advanced open source computational
693 framework for the propagation and interaction of two-phase mass flows, *Geosci. Model Dev.*, 10, 553–569,
694 <https://doi.org/10.5194/gmd-10-553-2017>, 2017.

695 Mergili, M., Emmer, A., Juřicová, A., Cochachin, A., Fischer, J.-T., Huggel, C., and Pudasaini, S.P.: How well can we
696 simulate complex hydro-geomorphic process chains? The 2012 multi-lake outburst flood in the Santa Cruz Valley
697 (Cordillera Blanca, Perú), *Earth Surf. Process. Landf.*, 43(7), 1373–1389, <https://doi.org/10.1002/esp.4318>, 2018a.

698 Mergili, M., Frank, B., Fischer, J.-T., Huggel, C., and Pudasaini, S. P.: Computational experiments on the 1962 and
699 1970 landslide events at Huascarán (Peru) with r.avaflow: Lessons learned for predictive mass flow simulations, *Geo-*
700 *morphology*, 322, 15–28, <https://doi.org/10.1016/j.geomorph.2018.08.032>, 2018b.

701 Mergili, M., Jaboyedoff, M., Pullarello, J., and Pudasaini, S. P.: Back-calculation of the 2017 Piz Cengalo-Bondo land-
702 slide cascade with r.avaflow, *Nat. Hazards Earth Syst. Sci. Discuss.*, <https://doi.org/10.5194/nhess-2019-204>, in review,
703 2019.

704 Nessler, H., and Tadmor, E.: Non-oscillatory central differencing for hyperbolic conservation laws, *J. Comput.*
705 *Phys.*, 87, 408–463, [https://doi.org/10.1016/0021-9991\(90\)90260-8](https://doi.org/10.1016/0021-9991(90)90260-8), 1990.

706 Ojeda, N.: Consolidación laguna Palcacocha, ELECTROPERU S.A., Unidad de glaciología y seguridad de lagunas,
707 Huaráz, Peru, 1974.

708 Oppenheim, V.: Sobre las Lagunas de Huaráz, *Boletín de la Sociedad Geológica del Perú*, 19, 68–80, 1946.

709 Pitman, E.B., and Le, L.: A two-fluid model for avalanche and debris flows. *Philos. Trans. R. Soc. A*, 363, 1573–1601,
710 <https://doi.org/10.1098/rsta.2005.1596>, 2005.

711 Portocarrero, C.: Seminario desastres naturales – geología, causas, efectos y prevenciones, ELECTROPERU S.A., Unidad
712 de glaciología y seguridad de lagunas, Huaráz, Peru, 1984.

713 Portocarrero, C.: The Glacial Lake Handbook: Reducing Risk from Dangerous Glacial Lakes in the Cordillera Blanca,
714 Peru, Technical Report, United States Agency for International Development, Global Climate Change Office, Climate
715 Change Resilient Development Project, Washington D.C., 2014.

716 Pudasaini, S. P.: A general two-phase debris flow model, *J. Geophys. Res. Earth Surf.*, 117, F03010,
717 <https://doi.org/10.1029/2011JF002186>, 2012.

718 Pudasaini, S. P.: A full description of generalized drag in mixture mass flows, *Phys. Fluids*, submitted manuscript,
719 2019a.

720 Pudasaini, S. P.: A fully analytical model for virtual mass force in mixture flows, *Int. J. Multiph. Flow*, 113, 142–152,
721 <https://doi.org/10.1016/j.ijmultiphaseflow.2019.01.005>, 2019b.

722 Pudasaini, S. P., and Hutter, K.: *Avalanche Dynamics: Dynamics of rapid flows of dense granular avalanches*, Springer,
723 2007.

724 Pudasaini, S. P., and Krautblatter, M.: A two-phase mechanical model for rock-ice avalanches, *J. Geophys. Res. Earth*
725 *Surf.*, 119, <https://doi.org/10.1002/2014JF003183>, 2014.

726 Pudasaini, S. P., and Fischer, J.-T.: A mechanical model for phase-separation in debris flow, arXiv:1610.03649, 2016a.

727 Pudasaini, S.P., and Fischer, J.-T.: A mechanical erosion model for two-phase mass flows, arXiv:1610.01806, 2016b.

728 Pudasaini, S.P., and Mergili, M.: A Multi-Phase Mass Flow Model, *J. Geophys. Res. Earth Surf.*, **JGRF21102**,
729 <https://doi.org/10.1029/2019JF005204>, 2019.

730 R Core Team: R: A Language and Environment for Statistical Computing, R Foundation for Statistical Computing,
731 Vienna, Austria, <https://www.r-project.org/>, last access: 4 February 2019.

732 Reynolds, J. M.: Managing the risks of glacial flooding at hydro plants, *Hydro Rev. Worldwide*, 6(2), 18–22, 1998.

733 Reynolds, J. M., Dolecki, A., and Portocarrero, C.: The construction of a drainage tunnel as part of glacial lake hazard
734 mitigation at Hualcán, Cordillera Blanca, Peru, in: Maund, J., and Eddleston, M. (eds.), *Geohazards in engineering*
735 *geology*, Geological Society Engineering Group Special Publication, 15, 41–48, 1998.

736 Richardson, S. D., and Reynolds, J. M.: An overview of glacial hazards in the Himalayas, *Quat. Int.*, 65/66, 31–47,
737 [https://doi.org/10.1016/S1040-6182\(99\)00035-X](https://doi.org/10.1016/S1040-6182(99)00035-X), 2000.

738 Rivas, D. S., Somos-Valenzuela, M. A., Hodges, B.R., and McKinney, D. C.: Predicting outflow induced by moraine
739 failure in glacial lakes: the Lake Palcacocha case from an uncertainty perspective, *Nat. Hazards Earth Syst. Sci.*, 15,
740 1163–1179, <https://doi.org/10.5194/nhess-15-1163-2015>, 2015.

741 Sattar, A., Goswami, A., and Kulkarni, A. V.: Application of 1D and 2D hydrodynamic modeling to study glacial lake
742 outburst flood (GLOF) and its impact on a hydropower station in Central Himalaya, *Nat. Hazards*, 97(2), 535–553,
743 <https://doi.org/10.1007/s11069-019-03657-6>, 2019a.

744 Sattar, A., Goswami, A., and Kulkarni, A. V.: Hydrodynamic moraine-breach modeling and outburst flood routing-A
745 hazard assessment of the South Lhonak lake, Sikkim, *Sci. Tot. Env.*, 668, 362–378,
746 <https://doi.org/10.1016/j.scitotenv.2019.02.388>, 2019b.

747 Savage, S. B., and Hutter, K.: The motion of a finite mass of granular material down a rough incline, *J. Fluid Mech.*,
748 199, 177–215, <https://doi.org/10.1017/S0022112089000340>, 1989.

749 Schaub, Y., Huggel, C., and Cochachin, A.: Ice-avalanche scenario elaboration and uncertainty propagation in numeri-
750 cal simulation of rock-/ice-avalanche-induced impact waves at Mount Hualcán and Lake 513, Peru, *Landslides*, 13,
751 1445–1459, <https://doi.org/10.1007/s10346-015-0658-2>, 2016.

752 Schneider, D., Huggel, C., Cochachin, A., Guillén, S., and García, J.: Mapping hazards from glacier lake outburst floods
753 based on modelling of process cascades at Lake 513, Carhuaz, Peru, *Adv. Geosci.*, 35, 145–155,
754 <https://doi.org/10.5194/adgeo-35-145-2014>, 2014.

755 Somos-Valenzuela, M. A., Chisolm, R. E., Rivas, D. S., Portocarrero, C., and McKinney, D. C.: Modeling a glacial lake
756 outburst flood process chain: the case of Lake Palcacocha and Huaráz, Peru, *Hydrol. Earth Syst. Sci.*, 20, 2519–2543,
757 <https://doi.org/10.5194/hess-20-2519-2016>, 2016.

758 Tai, Y. C., Noelle, S., Gray, J. M. N. T., and Hutter, K.: Shock-capturing and front-tracking methods for granular ava-
759 lanches, *J. Comput. Phys.*, 175(1), 269–301, <https://doi.org/10.1006/jcph.2001.6946>, 2002.

760 Takahashi, T., Nakagawa, H., Harada, T., and Yamashiki, Y.: Routing debris flows with particle segregation, *J. Hy-
761 draul. Res.*, 118, 1490–1507, [https://doi.org/10.1061/\(ASCE\)0733-9429\(1992\)118:11\(1490\)](https://doi.org/10.1061/(ASCE)0733-9429(1992)118:11(1490)), 1992.

762 Turzewski, M. D., Huntington, K. W., and LeVeque, R. J.: The geomorphic impact of outburst floods: Integrating ob-
763 servations and numerical simulations of the 2000 Yigong flood, eastern Himalaya, *J. Geophys. Res. Earth Surf.*,
764 <https://doi.org/10.1029/2018JF004778>, 2019.

765 Vilímek, V., Zapata, M. L., Klimeš, J., Patzelt, Z., and Santillán, N.: Influence of glacial retreat on natural hazards of
766 the Palcacocha Lake area, Peru, *Landslides*, 2(2), 107–115, <https://doi.org/10.1007/s10346-005-0052-6>, 2005.

767 Voellmy, A.: Über die Zerstörungskraft von Lawinen, *Schweizerische Bauzeitung*, 73, 159–162, 212–217, 246–249,
768 280–285, 1955.

769 Walder, J. S., and O'Connor, J. E.: Methods for predicting peak discharge of floods caused by failure of natural and
770 constructed earthen dams, *Water Resour. Res.*, 33(10), 2337–2348, <https://doi.org/10.1029/97WR01616>, 1997.

- 771 Wegner, S. A.: Lo Que el Agua se Llevó: Consecuencias y Lecciones del Aluvión de Huaráz de 1941, Technical Note 7
772 of the series “Technical Notes on Climate Change”, Ministry of Environment, Lima, Peru, 2014.
- 773 Wang, Y., Hutter, K., and Pudasaini, S. P.: The Savage-Hutter theory: A system of partial differential equations for
774 avalanche flows of snow, debris, and mud, ZAMM – J. Appl. Math. Mech., 84(8), 507–527,
775 <https://doi.org/10.1002/zamm.200310123>, 2004.
- 776 Westoby, M. J., Glasser, N. F., Brasington, J., Hambrey, M. J., Quincey, D. J., and Reynolds, J. M.: Modelling outburst
777 floods from moraine-dammed glacial lakes, Earth-Sci. Rev., 134, 137–159,
778 <https://doi.org/10.1016/j.earscirev.2014.03.009>, 2014.
- 779 Worni, R., Huggel, C., Clague, J. J., Schaub, Y., and Stoffel, M.: Coupling glacial lake impact, dam breach, and flood
780 processes: A modeling perspective, Geomorphology, 224, 161–176, <https://doi.org/10.1016/j.geomorph.2014.06.031>,
781 2014.
- 782 Zapata, M. L.: Lagunas con obras de seguridad en la Cordillera Blanca, INGEOMIN, glaciología y seguridad de lagunas,
783 Huaráz, Peru, 1978.
- 784 Zapata, M. L., Gómez, R. J. L., Santillán, N. P., Espinoza, H. V., and Huamaní, A.H.: Evaluación del estado de los glaci-
785 ares en la cabecera de la laguna Palcacocha, Informe técnico, INRENA, INGEMMET, Huaráz, Peru, 2003.

786

787 **Tables**

788 Table 1. Characteristics of Lake Palcacocha (1941 and 2016) and Lake Jircacocha (1941), and changes due to the 1941
 789 GLOF. Topographic reconstruction according to field observations, historic photographs, Vilímek et al. (2005), ANA
 790 (2016).

Parameter	Lake Palcacocha at 1941 GLOF	Lake Palcacocha 2016	Lake Jircacocha at 1941 GLOF
Lake level elevation (m a.s.l.)	4,610	4,563	~4,130
Surface area (10^3 m ²)	303	514	215
Lake volume (10^6 m ³)	12.9 ¹⁾	17.4	3.3
GLOF volume (10^6 m ³)	10.9 ²⁾	–	3.3
Max. lake depth (m)	108 ³⁾	71	33
Lowering of lake level (m)	47 ²⁾	–	33

791 ¹⁾ Reference values differ among sources: according to Vilímek et al. (2005), the volume of Lake Palcacocha in 1941
 792 was 9–11 million m³, whereas a reconstruction of ANA resulted in 13.1 million m³. In contrast, Vilímek et al. (2005)
 793 estimate a pre-failure volume of 4.8 million m³ for Lake Jircacocha, whereas, according to ANA, the volume was only
 794 3.0 million m³.

795 ²⁾ Computed from the difference between the pre-1941 lake level and the modern lake level (before mitigation) of
 796 4563 m. A reconstruction of ANA in 1948 resulted in in a residual lake volume of approx. 100,000 m³ and a residual
 797 depth of 17 m, both much smaller than derived through the reconstruction in the present work. One of the reasons for
 798 this discrepancy might be the change of the glacier in the period 1941–1948.

799 ³⁾ This value is highly uncertain and might represent an overestimation: the maximum depth of the lake strongly de-
 800 pends on the exact position of the glacier terminus, which was most likely located in an area of increasing lake depth
 801 in 1941.

802

803 Table 2. Reference information used for back-calculation of the 1941 process chain.

Parameter	Value	Remarks	References
Impact area	4.3 km ² ¹⁾	Mapped from post-event aerial images	Servicio Aerofotogramétrico Nacional
Breach volume – Palcacocha	2.0 million m ³	Comparison of pre- and post-event DTMs	Topographic reconstruction (Sect. 4)
Breach depth – Palcacocha	76 m	Elevation change at reference point R1 (Fig. 4)	Topographic reconstruction (Sect. 4)
Breach volume – Jircacocha	2.8 million m ³	Comparison of pre- and post-event DTMs	Topographic reconstruction (Sect. 4)
Material entrained upstream from Lake Jircacocha	1.0 million m ³	Maximum, value might be much lower	Topographic reconstruction (Sect. 4)
Material entrained downstream from Lake Jircacocha	3.1 million m ³	Maximum, value might be much lower	Topographic reconstruction (Sect. 4)
Material entrained in promontory	7.3 million m ³	Maximum, value might be much lower	Topographic reconstruction (Sect. 4)
Maximum depth of entrainment in promontory	50 m	Rough estimate	Somos-Valenzuela et al. (2016)
Material arriving at Huaráz	4–6 million m ³		Kaser and Georges (2003)

804 ¹⁾ Includes the surface of Lake Palcacocha

805

806 Table 3. Key model parameters applied to the simulations in the present work. Where three values are given, the first
 807 value applies to the glacier, the second value to the remaining area upstream of the dam of Lake Jircacocha, and the
 808 third value to the area downstream of the dam of Lake Jircacocha.

Symbol	Parameter	Unit	Value
ρ_s	Solid material density (grain density)	kg m ⁻³	2,700
ρ_f	Fluid material density	kg m ⁻³	1,000 ¹⁾
φ	Internal friction angle	Degree	28
δ	Basal friction angle	Degree	6, 12, 7
ν	Kinematic viscosity of fluid	m ² s ⁻¹	~0
τ_y	Yield strength of fluid	Pa	0 ²⁾
C_{AD}	Ambient drag coefficient	–	0.02, 0.005, 0.005
C_{FF}	Fluid friction coefficient	–	0.001, 0.004, 0.004
C_E	Entrainment coefficient	–	10 ^{-6.75 3)} , 10 ^{-7.15 4)}

809 ¹⁾ The fluid material density is set to 1,100 kg m⁻³ in Scenario AX.

810 ²⁾ The yield strength of the fluid phase is set to 5 Pa in Scenario AX.

811 ³⁾ This value applies to the dam of Lake Palcacocha.

812 ⁴⁾ This value applies to all other areas.

813

814 Table 4. Empirical relationships for the peak discharge in case of breach of moraine and landslide dams (Walder and
815 O'Connor, 1997), and the peak discharges estimated for Lake Palcacocha and Lake Jircacocha. q_p = peak discharge
816 ($\text{m}^3 \text{s}^{-1}$), V = total volume of water passing through the breach (m^3); D = drop of lake level (m); REG = regression;
817 ENV = envelope. The values of V and D for the two lakes are summarized in Table 1. See also Rivas et al. (2015).

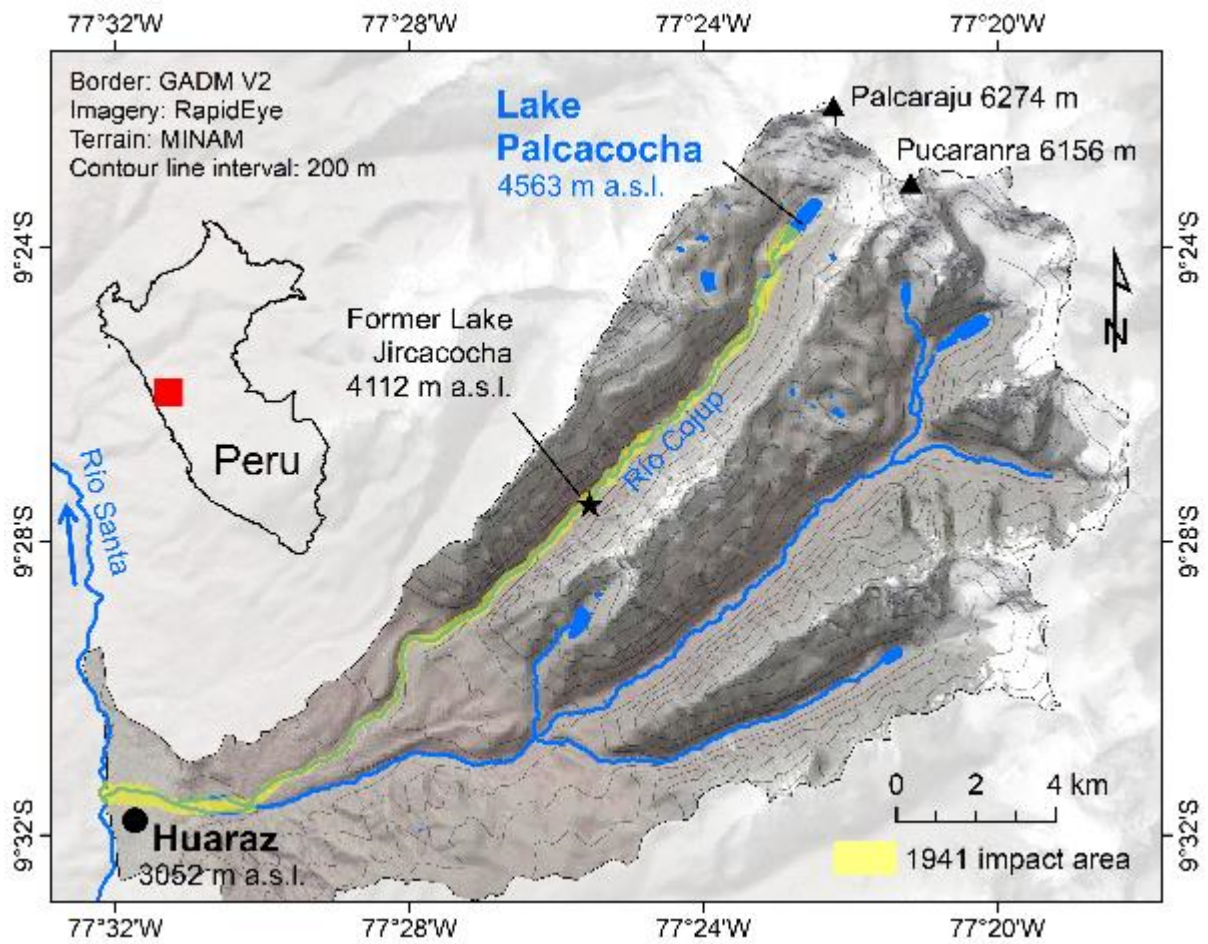
Moraine	a_{REG}	a_{ENV}	b	q_p Palcacocha REG ($\text{m}^3 \text{s}^{-1}$)	q_p Palcacocha ENV ($\text{m}^3 \text{s}^{-1}$)
$q_p = a \cdot V^b$	0.045	0.22	0.66	2,231	10,905
$q_p = a \cdot D^b$	60.3	610	0.84	1,531	15,484
$q_p = a \cdot (V \cdot D)^b$	0.19	1.1	0.47	2,560	14,819
Landslide	a_{REG}	a_{ENV}	b	q_p Jircacocha REG ($\text{m}^3 \text{s}^{-1}$)	q_p Jircacocha ENV ($\text{m}^3 \text{s}^{-1}$)
$q_p = a \cdot V^b$	1.6	46	0.46	1,638	47,101
$q_p = a \cdot D^b$	6.7	200	1.73	2,839	84,734
$q_p = a \cdot (V \cdot D)^b$	0.99	25	0.4	1,662	41,973

818

819 Table 5. Summary of the key results obtained with the computational experiments A–C. Refer to Tables 1 and 2 for the
 820 volumes involved, and to Table 4 for empirically expected peak discharges. Note that all entrained volumes are com-
 821 posed of 80% of solid and 20% of fluid material in terms of volume.

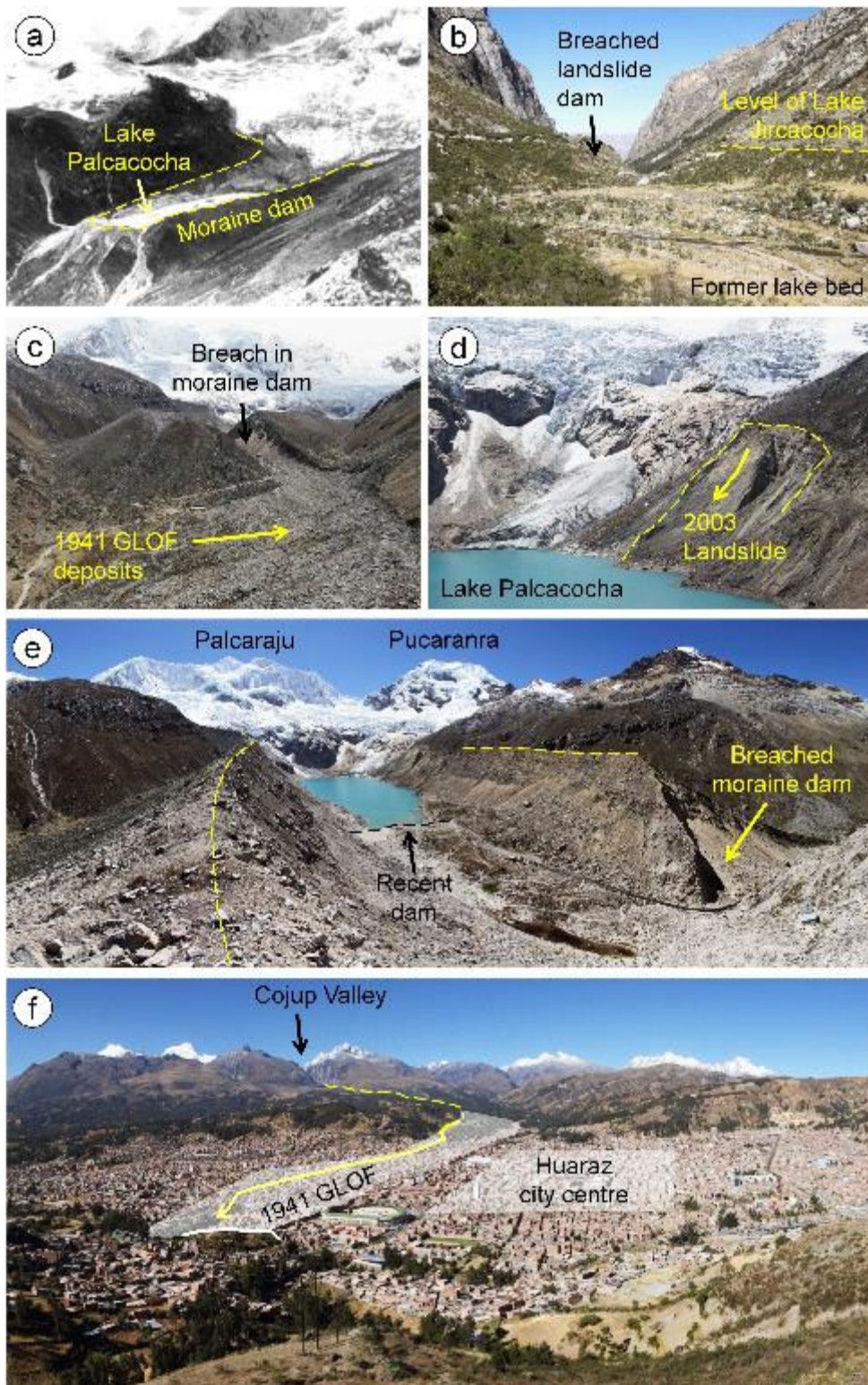
Scenario	A	AX	B	C
Description	Overtopping	Overtopping	Impact wave	Dam collapse
Entrained volume Lake Palcacocha dam (m ³)	1.5 million	1.4 million	2.7 million	–
Fluid peak discharge at outlet of Lake Palcacocha (m ³ s ⁻¹)	19,000	8,200	17,000 ¹⁾	38,000
Entrained volume Lake Jircacocha dam (m ³)	2.2 million	2.0 million	2.2 million	2.2 million
Fluid peak discharge at outlet of Lake Jircacocha (m ³ s ⁻¹)	14,700	7,600	15,000	15,400
Material entrained up-stream from Lake Jircacocha (m ³)	0.7 million	0.7 million	0.7 million	0.7 million
Material entrained down-stream from Lake Jircacocha (m ³)	1.5 million	1.3 million	1.5 million	1.5 million
Material entrained in promontory (m ³)	5.3 million	5.3 million	5.3 million	5.3 million
Travel time to Huaráz (s) Start (Peak)	2,760 (3,660)	4,200 (6,480)	3,060 (4,080)	2,160 (3,060)
Solid delivered to Huaráz (m ³)	2.5 million	2.6 million	2.5 million	2.7 million

822 ¹⁾ Peak of initial overtopping as response to the impact wave: 7,000 m³ s⁻¹



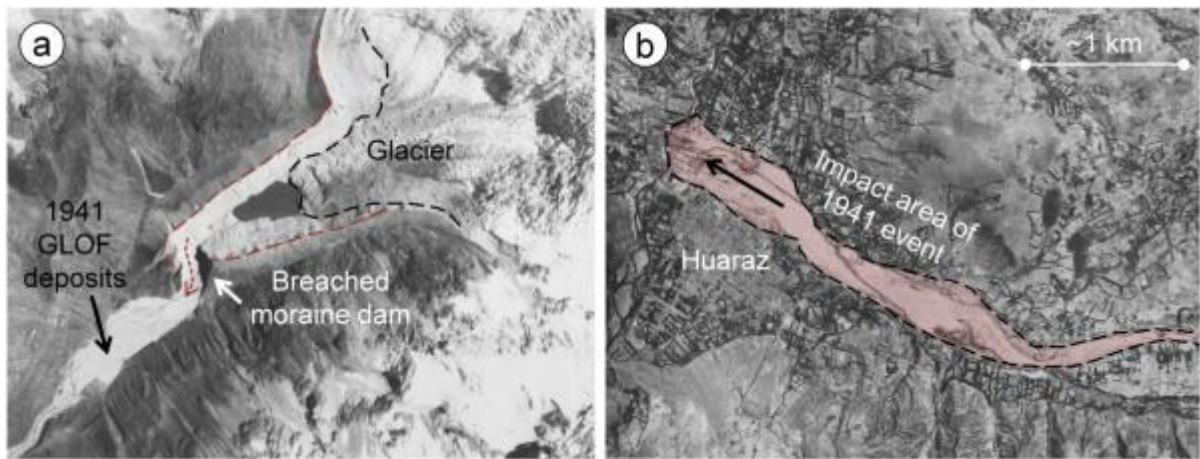
824
825 Fig. 1. Location and main geographic features of the Quilcay catchment with Lake Palcacocha and the former Lake
826 Jircacocha.

827

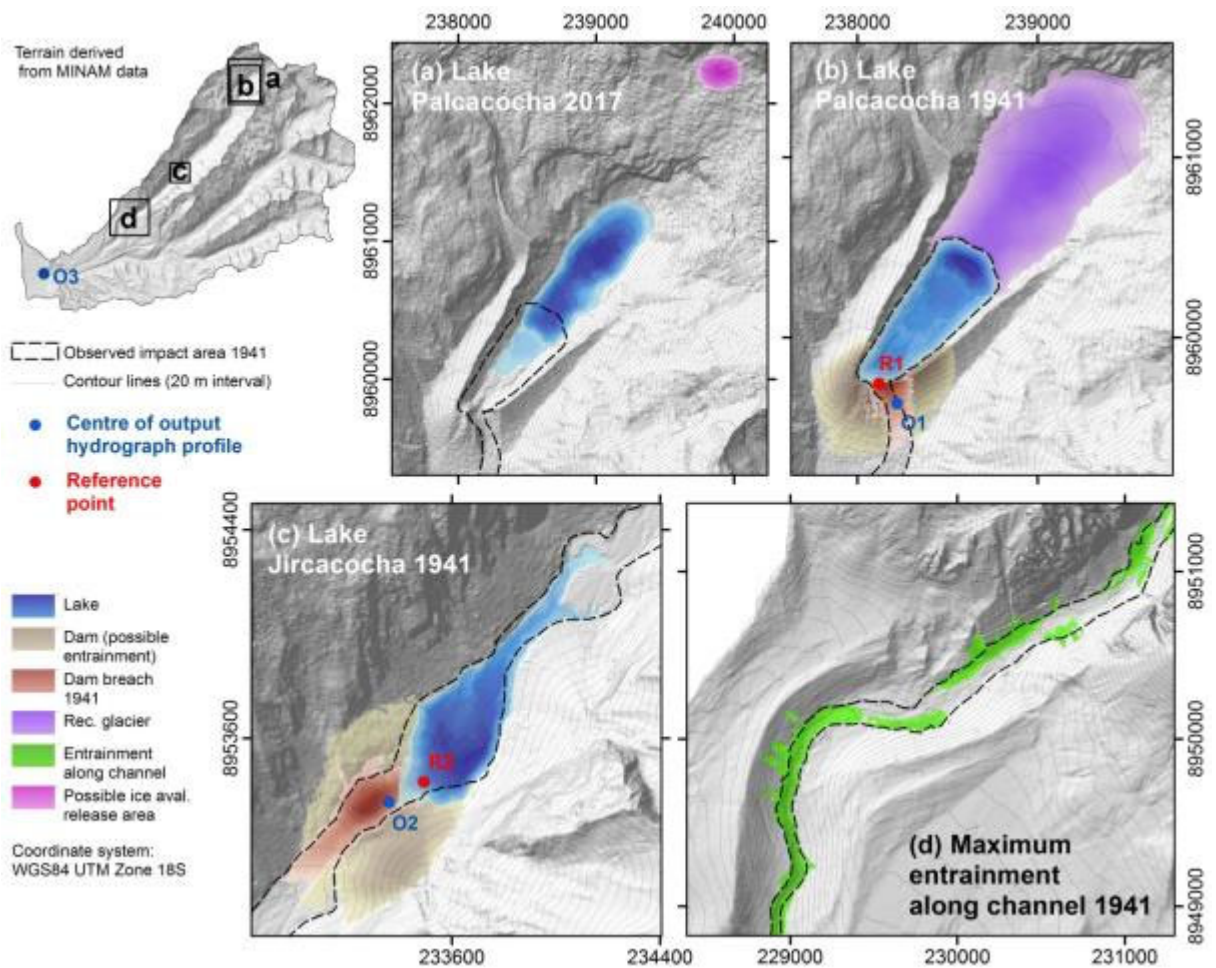


828
 829 Fig. 2. The Quilcay catchment from Lake Palcacocha down to Huaráz. (a) Lake Palcacocha in 1939, two years prior to
 830 the 1941 event. (b) The site of former Lake Jircacocha with the breached landslide dam and the former lake level. (c)
 831 Breached moraine dam and 1941 GLOF deposits, seen from downstream. (d) Left lateral moraine of Lake Palcacocha
 832 with landslide area of 2003. (e) Panoramic view of Lake Palcacocha, with the breach in the moraine dam and the
 833 modern lake impounded by a smaller terminal moraine and two artificial dams. (f) Panoramic view of Huaráz with
 834 city centre and approximate impact area of the 1941 event. **Note that a small part of the lowermost portion of the im-**
 835 **act area is hidden behind a hillslope.** Photos: (a) Hans Kinzl, 1939 (Kinzl and Schneider, 1950); (b) Martin Mergili,
 836 July 2017; (c) Gisela Eberhard, July 2018; (d)–(f): Martin Mergili, July 2017.

837

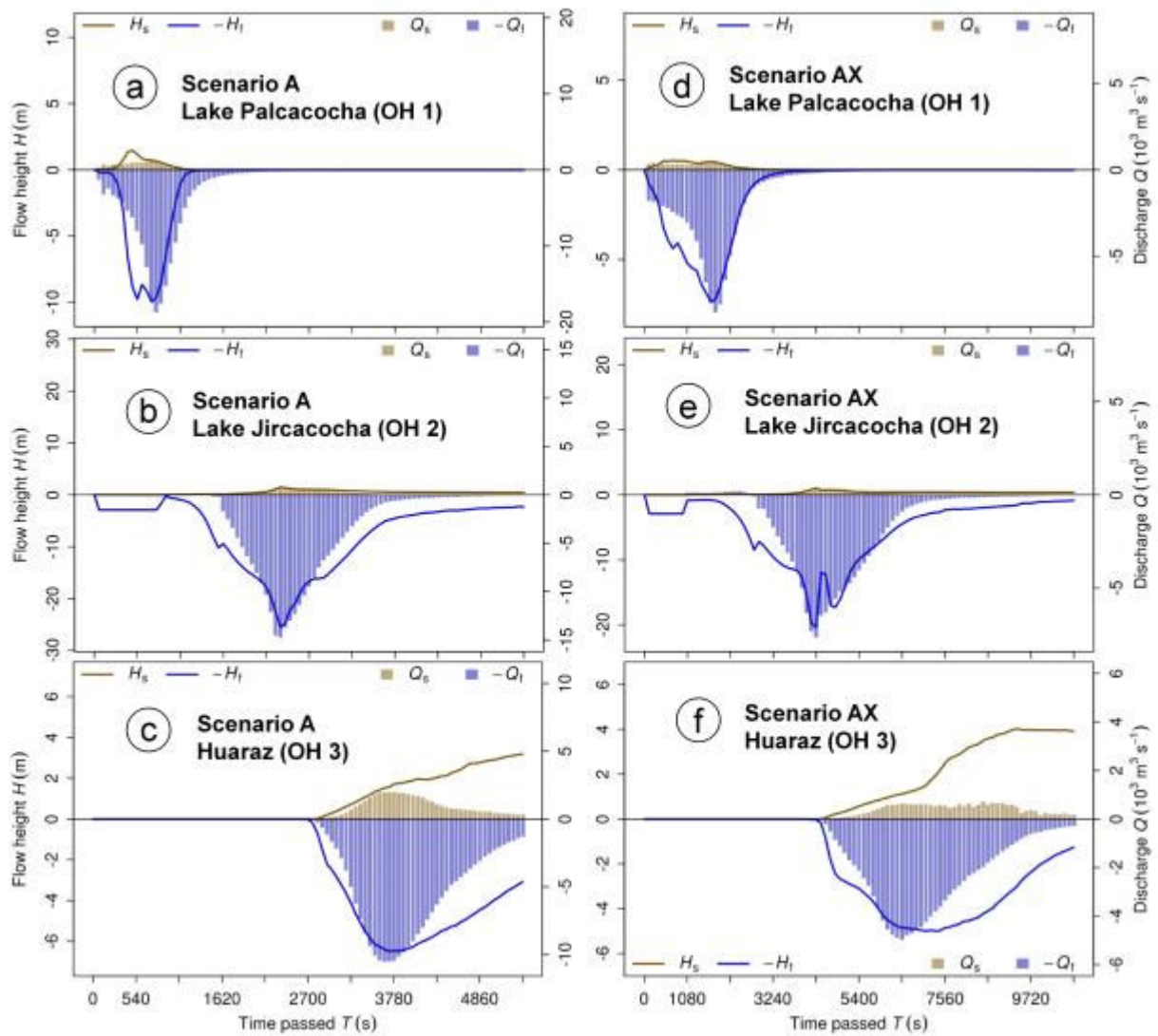


838
839 Fig. 3. Situation in 1948, seven years after the 1941 event. (a) Residual Lake Palcacocha, and traces of the 1941 event.
840 (b) Huaráz with the impact area of the 1941 event. Imagery source: Servicio Aerofotogramétrico Nacional, Perú.
841



842
843
844
845
846
847

Fig. 4. Reconstruction of lakes and topography. (a) Lake Palcacocha in 2017. (b) Lake Palcacocha before the 1941 event. (c) Lake Jircacocha before the 1941 event. (d) Part of the promontory section of the Cojup Valley, with lowering of the valley bottom by up to 50 m. The possible rock avalanche release area is shown in (a) for clarity, but is applied to the 1941 situation.



848

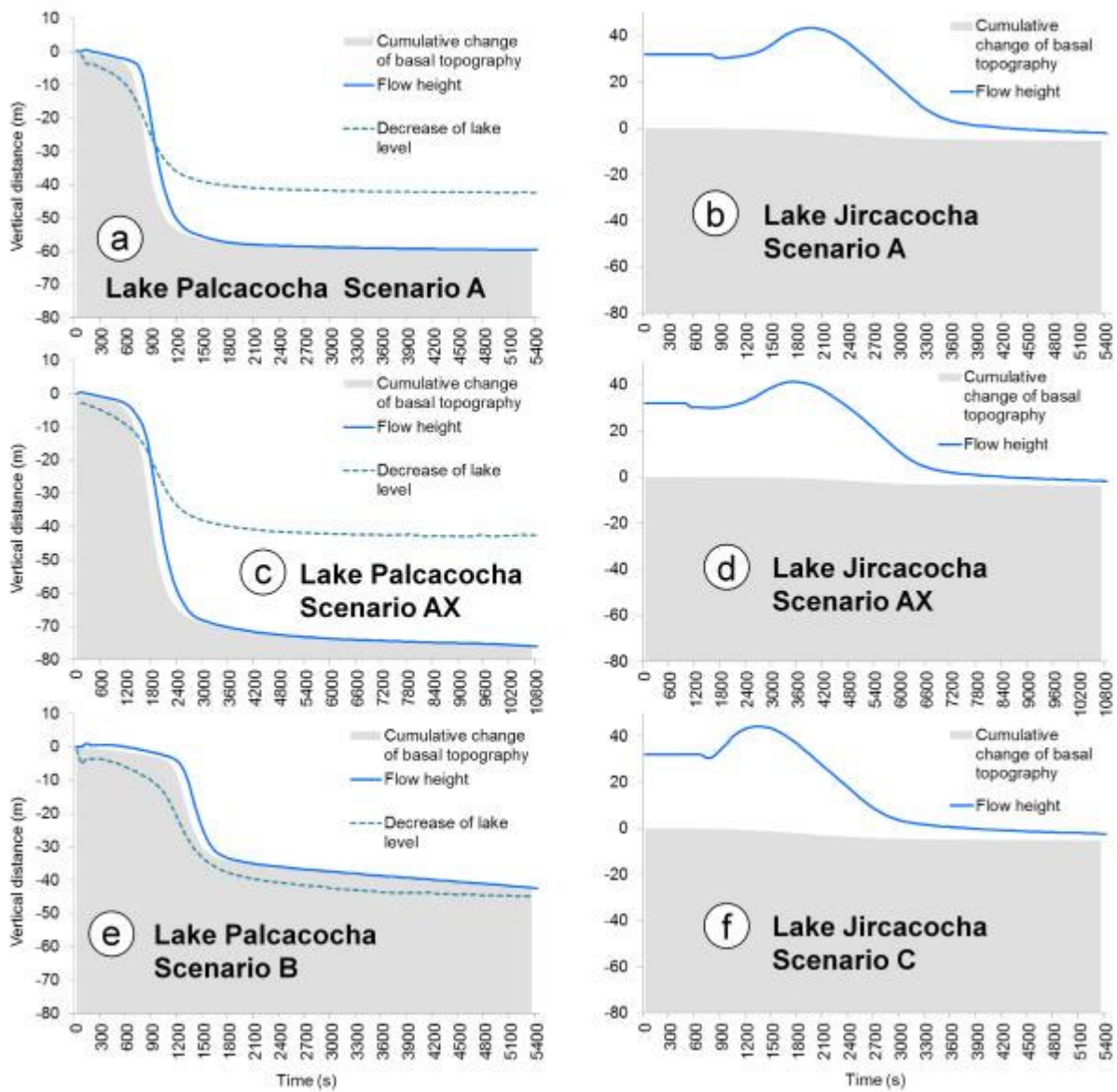
849

850

851

852

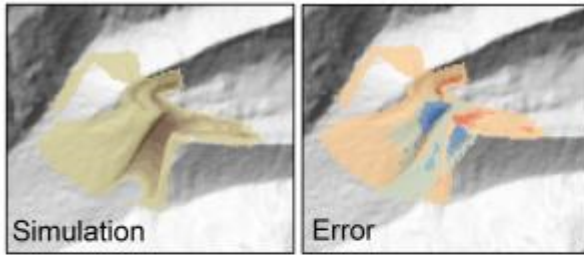
Fig. 5. Hydrographs of moraine dam failure of Lake Palcacocha (a, d), landslide dam failure of Lake Jircacocha (b, e), and the flow entering the urban area of Huaráz (c, f) for the scenarios A and AX. Note that, for clarity, fluid flow heights and discharges are plotted in negative direction.



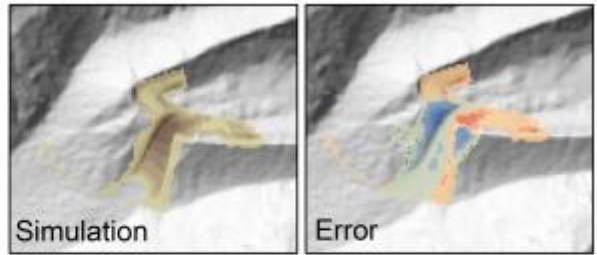
853
854
855
856
857
858
859
860
861
862
863

Fig. 6. Evolution of flow height and basal topography at the outlets of Lake Palcacocha (reference point R1 in Fig. 4b), and Lake Jircacocha (reference point R2 in Fig. 4c). The reference points are placed in a way to best represent the evolution of the breach in the dam for Lake Palcacocha, and the evolution of the impact wave for Lake Jircacocha. Additionally, the evolution of the lake level is shown for Lake Palcacocha. Note that the result for Scenario B is only displayed for Lake Palcacocha (e), whereas the result for Scenario C is only illustrated for Lake Jircacocha (f). The vertical distance displayed on the y axis refers to the terrain height or the lake level at the start of the simulation, respectively, whereby the flow height is imposed onto the topography. In Scenario B, the initial impact wave at the dam of Lake Palcacocha is only poorly represented due to the low temporal resolution of the simulation, and due to blurring by numerical effects (e).

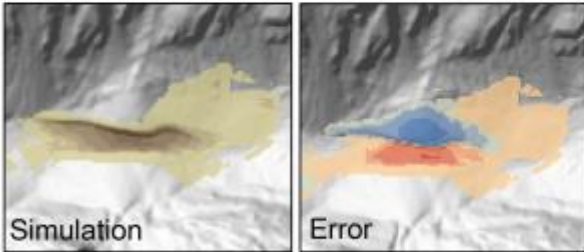
(a) Lake Palcacocha - Scenario A



(c) Lake Palcacocha - Scenario AX



(b) Lake Jircacocha - Scenario A



(d) Lake Jircacocha - Scenario AX

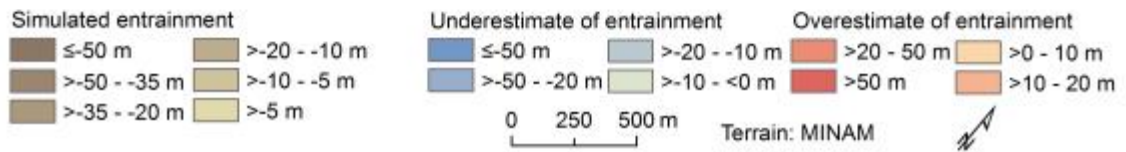
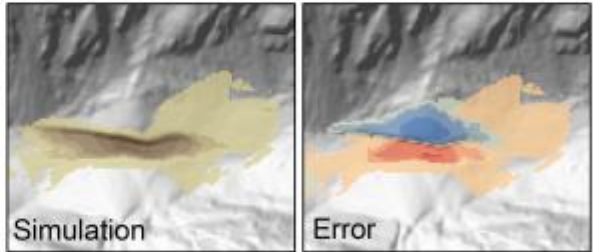
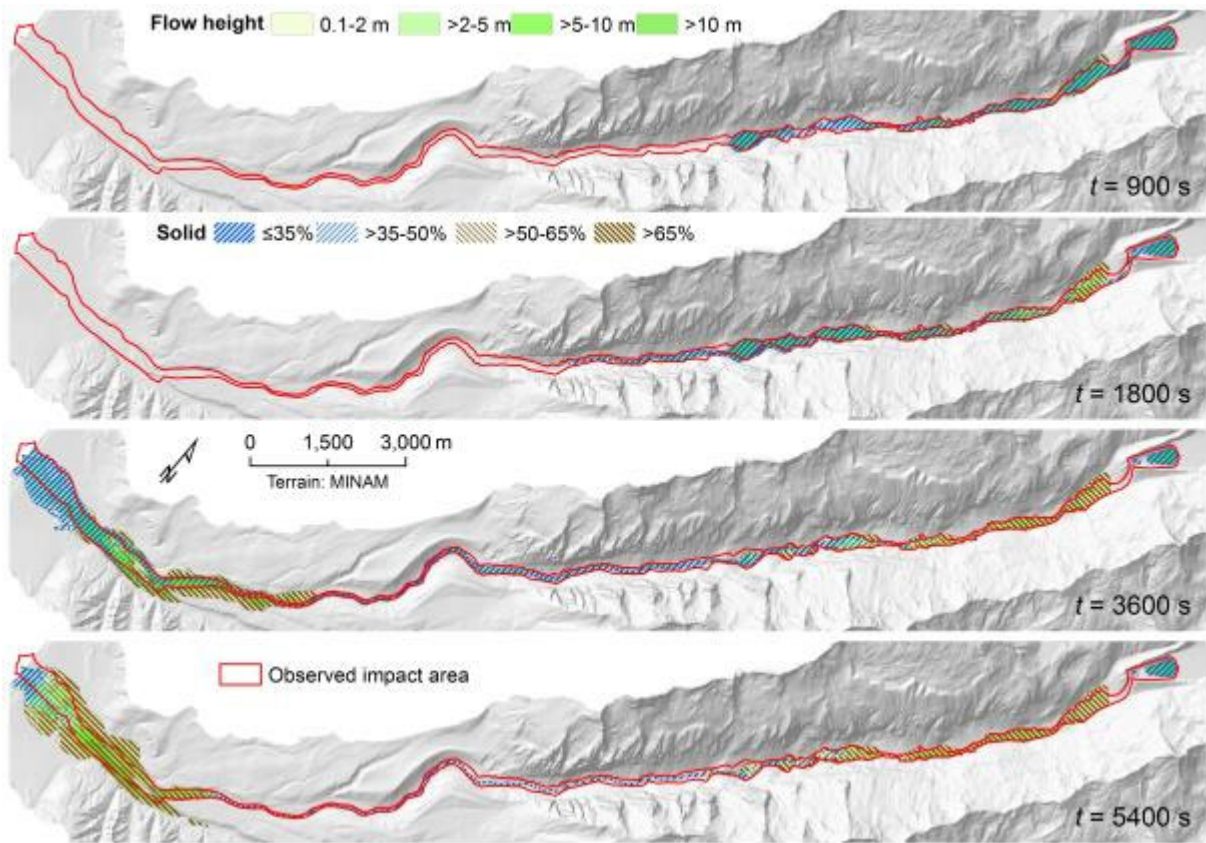
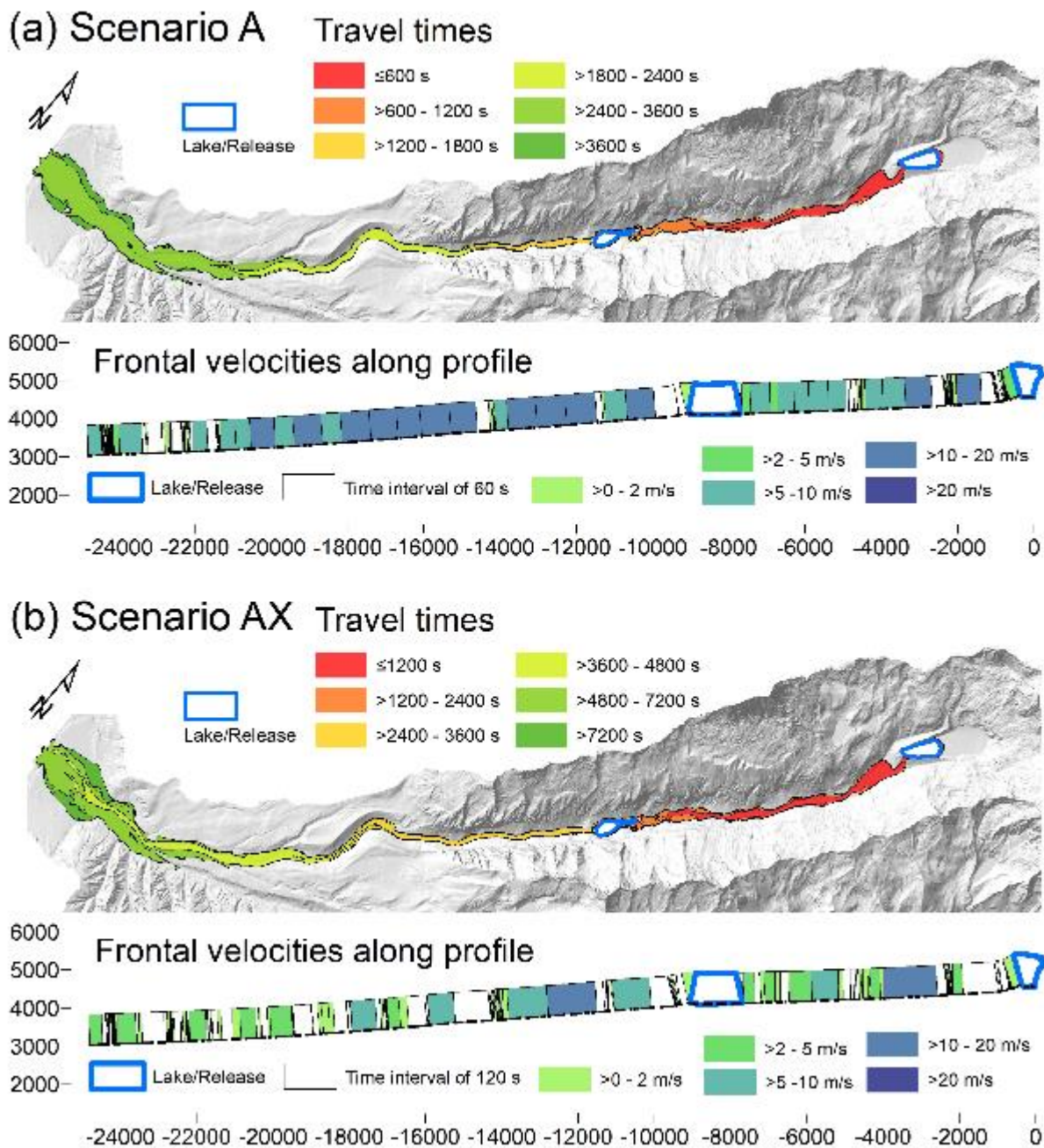


Fig. 7. Simulated versus reconstructed entrainment patterns for the scenarios A and AX. The total entrained height and the difference between simulated and reconstructed entrainment (error) are shown. (a) Lake Palcacocha, Scenario A. (b) Lake Jircacocha, Scenario A. (c) Lake Palcacocha, Scenario AX. (d) Lake Jircacocha, Scenario AX.



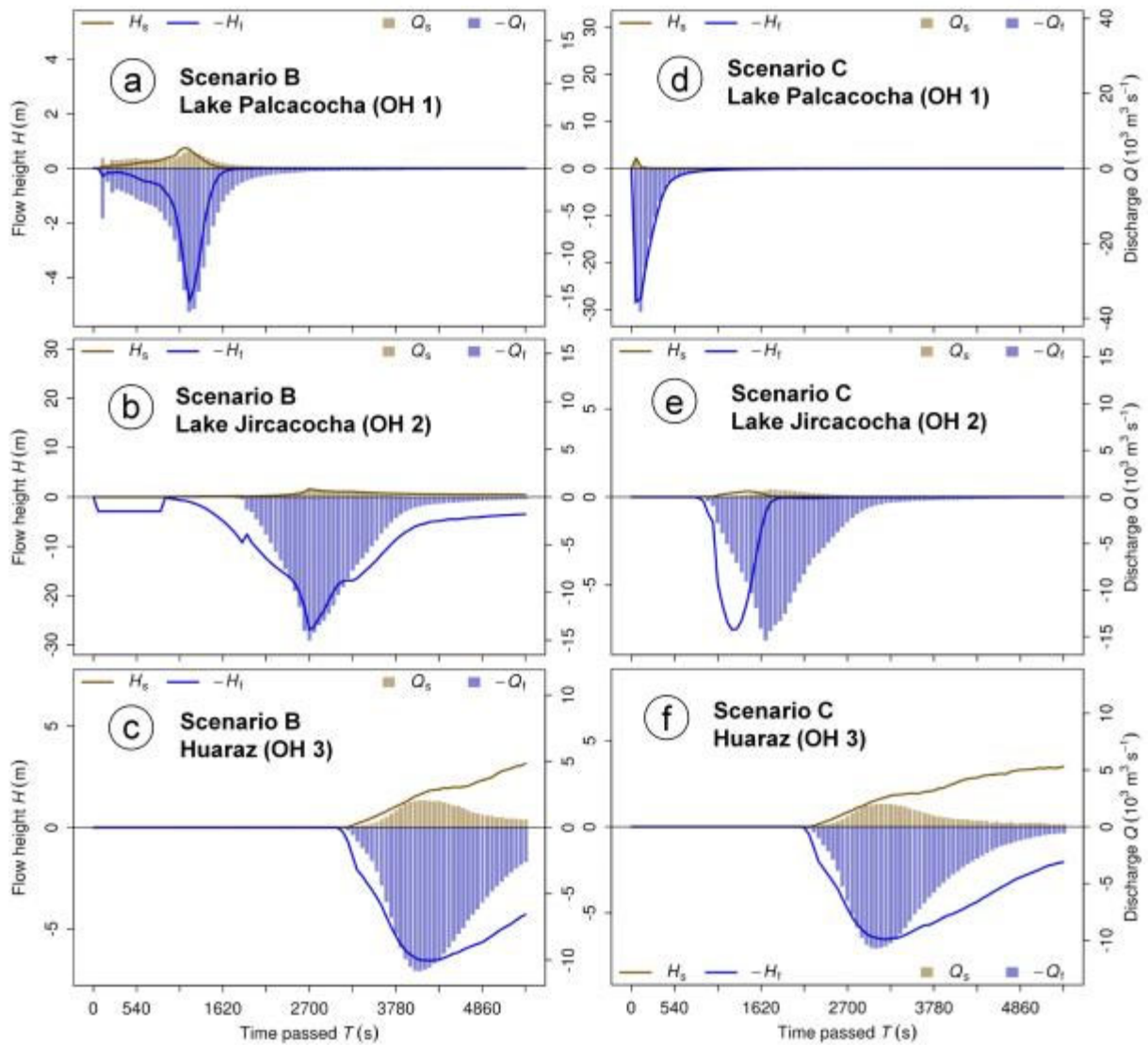
869
870
871

Fig. 8. Evolution of the flow in space and time (Scenario A).



872
873
874
875

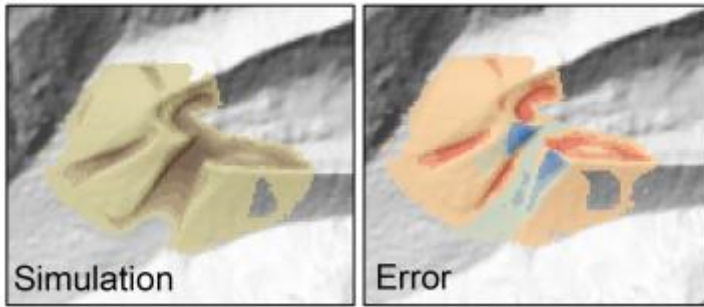
Fig. 9. Travel times and frontal velocities for the scenarios (a) A and (b) AX. Void fields in the profile graph refer to areas without clearly defined flow front.



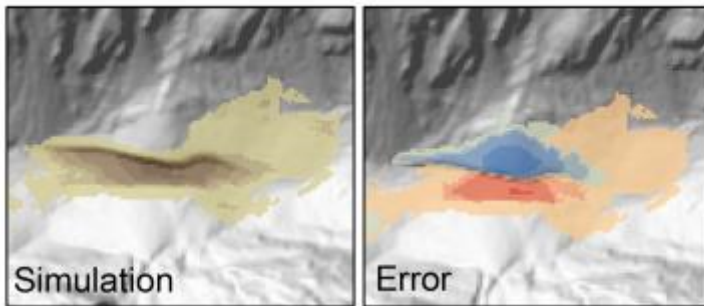
876
 877 Fig. 10. Hydrographs of moraine dam failure of Lake Palcacocha (a, d), landslide dam failure of Lake Jircacocha (b, e),
 878 and the flow entering the urban area of Huaráz (c, f) for the scenarios B and C. Note that, for clarity, fluid flow heights
 879 and discharges are plotted in negative direction.

880

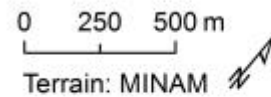
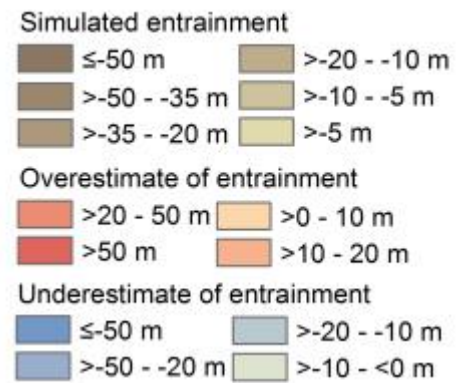
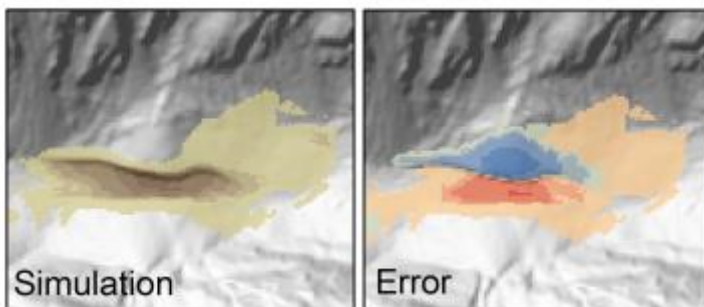
(a) Lake Palcacocha - Scenario B



(b) Lake Jircacocha - Scenario B

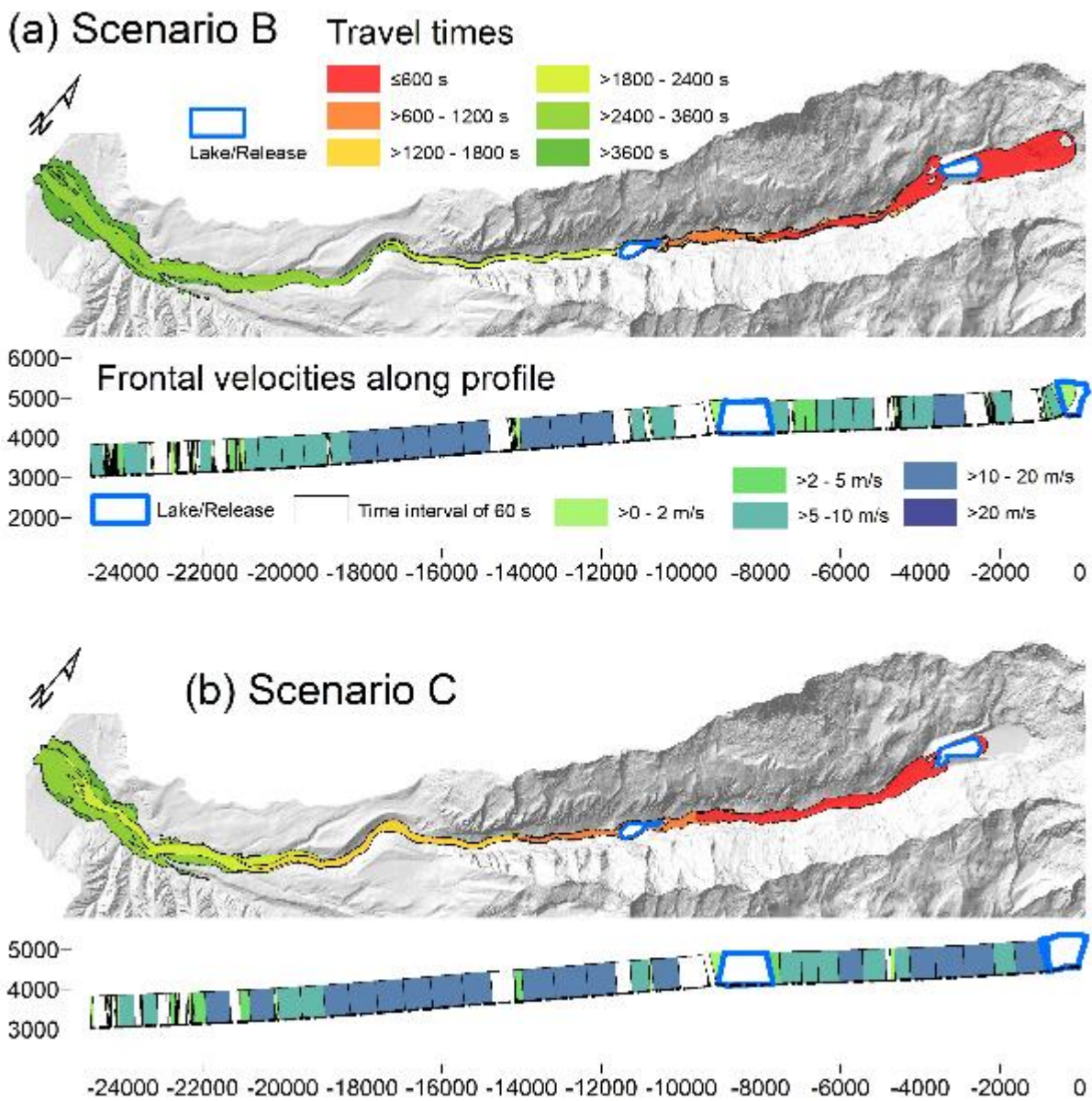


(c) Lake Jircacocha - Scenario C



881
882
883
884
885

Fig. 11. Simulated versus reconstructed entrainment patterns for the scenarios B and C. The total entrained height and the difference between simulated and reconstructed entrainment (error) are shown. (a) Lake Palcacocha, Scenario B. (b) Lake Jircacocha, Scenario B. (c) Lake Jircacocha, Scenario C.



886 Fig. 12. Travel times and frontal velocities for the scenarios (a) B and (b) C. Note that the legend of (a) also applies to
 887 (b). Void fields in the profile graph refer to areas without clearly defined flow front.
 888
 889